PHILOSOPHICAL TRANSACTIONS OF THE ROYAL SOCIETY A MATHEMATICAL, PHYSICAL & ENGINEERING SCIENCES

Dynamical Theory of Electron Diffraction for the Electron Microscopic Image of Crystal Lattices I. Images of Single Crystals

H. Hashimoto, M. Mannami and T. Naiki

Phil. Trans. R. Soc. Lond. A 1961 **253**, 459-489
doi: 10.1098/rsta.1961.0006

DYNAMICAL THEORY OF ELECTRON DIFFRACTION FOR THE ELECTRON MICROSCOPIC IMAGE OF CRYSTAL LATTICES

I. IMAGES OF SINGLE CRYSTALS

By H. HASHIMOTO,† M. MANNAMI‡ and T. NAIKI†

(*Communicated by A. H. Cottrell, F.R.S.—Received 9 April 1960*)

[Plates 5 and 6]

CONTENTS

The dynamical theory of electron diffraction is applied to the interpretation of electron microscopic images of lattice planes of plate- and wedge-shaped crystals. The wave functions and corresponding intensities predicting interference fringes on the exit surface of a crystal are derived. It is shown in both cases that the fringes are composed of parallel lines and the spacing of the fringes at the exact Bragg angle coincides with that of the original lattice but the positions of the lines do not coincide with those of potential maxima in the crystal, i.e. intensity profiles of the fringes do not represent the variation of mass-thickness in the crystal. The intensity profiles and the spacings of the fringes vary with the thickness of crystal and the deviation from the Bragg angle.

The fringes from a bent plate-shaped crystal, which are formed on the extinction contour bands, show the same spacing as that of the crystal lattice along the centre of the contour but they have an increased or decreased spacing near the edge of the contour. The fringes which are formed on the subsidiary extinction contour also show spacing anomaly; they are shifted by half the corresponding amount for the principal contour.

The spacing of the fringes of a wedge-shaped crystal coincides with that of the original lattice at the exact Bragg angle, but the contrast of the lines reverses wherever the thickness of the crystal increases by an amount of $\lambda E/2V_g$ (λ, wave length; E, accelerating potential; V_g, Fourier coefficient of inner potential of the crystal). For deviation from the Bragg angle, the spacing of the fringes, in general, does not coincide with that of the original lattice and, moreover, the contrast of the lines reverses wherever the thickness of the crystal increases by an amount of $\lambda E/V_g$.

The anomalies of spacing and reversal of contrast which are expected from the present theory were observed in the electron microscopic images of metal-phthalocyanine and sodium faujasite crystals respectively.

The effects of absorption by the crystal and divergence of illumination on the contrast of the image are discussed and the possibility of obtaining two-dimensional projections of the atomic arrangement in a crystal by using electron microscopic images is also discussed.

† Physical Institute, Kyoto Technical University, Kyoto, Japan.
‡ Physical Institute, Kyoto University, Kyoto, Japan.

1. Introduction

It is widely known that Menter (1956*a*) was the first to observe the images of the lattice plane $(20\bar{1})$ of Pt-phthalocyanine crystals (spacing $a_{(20\bar{1})} = 11{\cdot}9$ Å) and lattice planes $(20\bar{1})$, (001) of Cu-phthalocyanine crystal (spacing $a_{(20\bar{1})} = 9{\cdot}8$ Å, $a_{(001)} = 12{\cdot}4$ Å) with the electron microscope. After his observation, several authors observed the images of crystal lattices with the electron microscope; Labaw & Wyckoff (1957) observed indanthrene scarlet ($a = 15{\cdot}4$, $19{\cdot}3$ and $28{\cdot}1$ Å), Menter (1956*b*) sodium faujasite ($a = 14{\cdot}4$ Å), Bassett & Menter (1957) molybdenum trioxide ($a_{(020)} = 6{\cdot}93$ Å) and Neider (1956) Ni-phthalocyanine ($a_{(20\bar{1})} = 9{\cdot}8$ Å). Electron microscopic images of the super-lattice of antigorite ($a = 90$ Å) were also observed by Brindley, Comer, Uyeda & Zussman (1958) and Uyeda, Masuda, Tochigi, Ito & Yotsumoto (1958). Ogawa, Watanabe, Watanabe & Komoda (1958) observed the fringe of 20 Å spacing in the image of the ordered alloy of CuAu II.

The electron microscopic image of crystal lattices was discussed by Menter (1956*a*) on the basis of the kinematical theory of electron diffraction and Abbe's theory of image formation and it was concluded that the image should be equally spaced parallel fringes. He measured (Menter 1956*b*) the spacings of many fringes and showed that their average coincided with that of the original lattice. Uyeda (1955) suggested before Menter's observation that the image of the crystal lattice should be parallel lines. Niehrs (1954) discussed the lattice image of MgO smoke crystal at the exact Bragg condition by the dynamical theory of electron diffraction and concluded that the image at the wedge should be equally spaced parallel lines with stepped structure. Niehrs (1956) further discussed the image of resolved atoms in MgO smoke crystals. Uyeda (1957) reported briefly that, with increasing thickness of the wedge-shaped crystal, contrast of the image and the amount of the step will decrease due to the absorption of electrons in the crystal. Cowley (1959), by using the theory developed by his group, interpreted the image of crystal lattices with various thicknesses and suggested that a thin crystal may be represented as a phase grating but that for a thick crystal the dynamic scattering of electrons in the crystal must be considered, taking into account the amplitude-grating effect due to absorption. He suggested that for a crystal for example thinner than 100 Å, the image will appear not at exact focus but out of focus. He suggested, moreover, that the stepped structure observed in antigorite fringes is due to the simultaneous reflexion of electron waves. He indicated that the stepped structure of the fringes which appear on the exit surface of wedge-shaped crystals is also expected from his theory. Lentz & Scheffels (1958) also suggested that the contrast of the fringe of thin film with periodic structure is chiefly due to out-of-focus effects.

By using the dynamical theory of electron diffraction several authors have discussed the contrast in transmission electron micrographs of crystalline materials. But their interpretations were confined to the intensity of only the primary or reflected waves. Heidenreich (1949) and Hashimoto (1954) discussed the equal inclination fringes with subsidiary maxima which appear in the ordinary electron microscopic image and shadow electron microscopic image of bent crystalline film. Niehrs (1954), Hibi, Kambe & Honjo (1955) discussed the equal thickness fringes which appear in the electron microscopic image of a wedge-shaped crystal. Whelan & Hirsch (1957) discussed the intensity distribution of the

electron microscopic images of a plate-like crystal containing stacking faults. Whelan & Hirsch explained the intensity variation of the fringes by deviation from the Bragg angle and the variation of the thickness of the crystal.

In the course of the analysis of moiré fringes (Hashimoto 1958), one of the present authors supposed that the spacing anomaly will appear locally in the lattice image of a crystalline film where the Bragg condition is not exactly satisfied. Such spacing anomalies in the image were detected (Hashimoto & Yotsumoto 1959) in the micrographs of crystal lattices of Cu- Pt- and Zn-phthalocyanine and antigorite. In order to explain the spacing anomaly in the image in detail, it was found necessary to apply the dynamical theory of electron diffraction to the single bent crystalline film. In this paper, the theory is applied to the interpretation of the contrast of the image of single crystal lattices with different crystal habit, such as wedges or plates, in various orientations to the incident electron waves.

In §§ 2, 3 and 4 of this paper, the dynamical theory is applied to the Laue case and the wave functions and the corresponding intensities predicting interference fringes formed on the exit surface of the crystal are derived, the absorption of electron waves being neglected. In §§ 5 and 6 of this paper the absorption of electron waves and divergence of illumination are discussed. In § 7 numerical calculations are compared with experimental results, and the possibility of observing the atomic arrangement in crystals by using the electron microscopic images of the crystal lattice is also discussed.

In part II, application of the present theory to the interpretation of moiré fringes will be presented.

2. Wave functions corresponding to the image of lattice planes of plate-shaped crystals

According to Abbe's (1837) theory, the image of a crystal lattice is formed by the interference of the primary and reflected waves which have passed through the crystal. In this section, the wave function corresponding to the well focused image by an ideal lens and axial illumination is derived for the case of single Bragg reflexion. Functions for the primary and reflected waves from plate- and wedge-shaped crystals have already been derived by

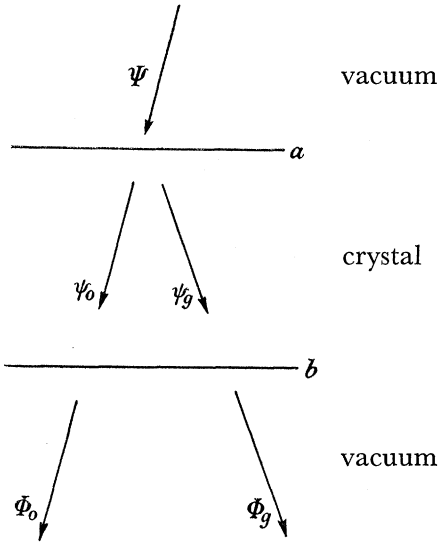

Figure 1. Waves in a vacuum and a crystal.

several workers using the dynamical theory of electron diffraction, developed by Bethe (1928). They are, in particular, MacGillavry (1940), Thomson & Cochrane (1939), Blackman (1939), Heidenreich (1949) and Kato (1952, 1953). In this section, Kato's theory is briefly outlined so that we may better understand the meaning of the notation and that of the wave functions inside and outside of the crystal. Afterwards, the wave function corresponding to the image of a crystal lattice is derived.

Let an electron wave,

$$\Psi(\mathbf{r}) = \Psi \exp 2\pi i(\mathbf{K}\cdot\mathbf{r}), \tag{1}$$

which is accelerated by an energy E, enter a crystal through surface a (incident surface) as shown in figure 1, where Ψ, $\mathbf{K}$ and $\mathbf{r}$ are the amplitude, wave vector and position vector of the wave respectively. Then two waves ψ_0 and ψ_g, which are the primary and reflected waves respectively, appear in the crystal if the crystal is at the Bragg angle.

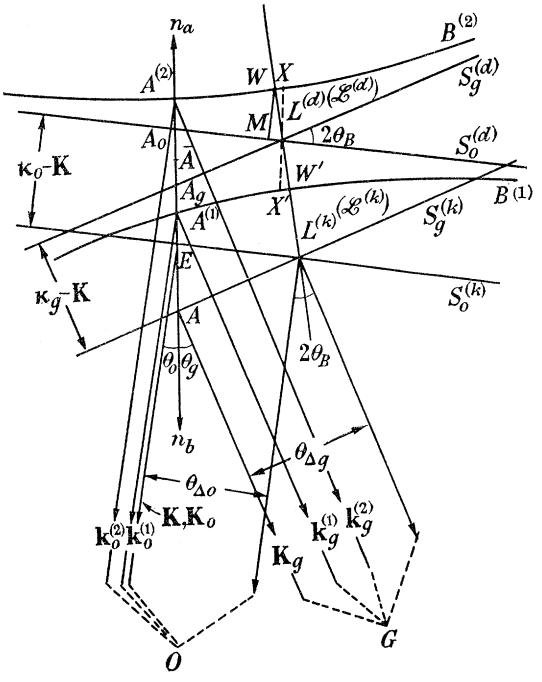

FIGURE 2. For legend see facing page.

The wave $\psi(\mathbf{r})$ appearing in the crystal of the potential $V(\mathbf{r})$ should satisfy the Schrödinger equation

$$\nabla^2\psi(\mathbf{r}) + \frac{8\pi^2 me}{h^2}[E + V(\mathbf{r})]\,\psi(\mathbf{r}) = 0, \tag{2}$$

where

$$\frac{2me}{h^2}V(\mathbf{r}) \equiv U(\mathbf{r}) = \sum_g U_g \exp 2\pi i(\mathbf{g}\cdot\mathbf{r}), \tag{3}$$

and $\mathbf{g}$ is the reciprocal lattice vector and all other symbols bear their usual significance.

As the solution of equation (2), $\psi(\mathbf{r})$ can be expressed as

$$\psi(\mathbf{r}) = \sum_g \psi_g \exp 2\pi i(\mathbf{k}_g\cdot\mathbf{r}), \tag{4}$$

where

$$\mathbf{k}_g = \mathbf{k}_0 + \mathbf{g}. \tag{5}$$

By substituting equations (3), (4) and (5) into (2), one arrives at a system of linear homogeneous equations. As a single Bragg reflexion is excited, only the amplitudes ψ_0 and ψ_g have appreciable values, then the equations become

$$\begin{pmatrix} \kappa_0^2 - \mathbf{k}_0^2 & U_{-g} \\ U_g & \kappa_g^2 - \mathbf{k}_g^2 \end{pmatrix} \begin{pmatrix} \psi_0 \\ \psi_g \end{pmatrix} = 0. \tag{6}$$

FIGURE 2. Dispersion surface and wave points for a plate-shaped crystal.

O and G, the origin and a reciprocal lattice point.
E, wave point of incident wave and transmitted primary wave.
A, wave point of the transmitted reflexion wave. The plane of this figure is determined by the vectors $\overrightarrow{EO} = \mathbf{K}$ and $\overrightarrow{OG} = \mathbf{g}$.
$S_0^{(k)}$, $S_0^{(d)}$ and $S_g^{(k)}$, $S_g^{(d)}$, spheres of large radius K and κ centred on O and G.
$L^{(k)}$ and $L^{(d)}$, kinematical and dynamical Laue circles, i.e. intersection of $S_0^{(k)}$ and $S_g^{(k)}$ and that of $S_0^{(d)}$ and $S_g^{(d)}$.
$\mathscr{L}^{(k)}$ and $\mathscr{L}^{(d)}$, kinematical and dynamical Laue points.
n_a, n_b, normals of entrance and exit surfaces. They do not lie on the plane of this figure in general.
$\angle OL^{(k)}G/2$, Bragg angle.
$\angle OEn_b = \theta_0$, the angle between n_b and $\mathbf{K}_0$.
$\angle GAn_b = \theta_g$, the angle between n_b and $\mathbf{K}_g$.
$\theta_{\Delta 0}$, deviation of the incident or primary wave vector from the Bragg angle.
$\theta_{\Delta g}$, deviation of the reflected wave vector from the Bragg angle.
$B^{(1)}$ and $B^{(2)}$, two branches of the dispersion surface, approximately hyperbolic surfaces whose asymptotic surfaces are $S_0^{(d)}$ and $S_g^{(d)}$.
$A^{(1)}$ and $A^{(2)}$, wave points of the crystal waves.
A_0 and A_g, intersection of $S_0^{(d)}$ and $n_a n_b$ and that of $S_g^{(d)}$ and $n_a n_b$.
$\bar{A}$, wave point of mean value of crystal waves, middle point of $A_0 A_g$.
W and W', intersections of Brillouin zone boundary and dispersion surface.
X and X', intersections of normal of crystal surface passing through $\mathscr{L}^{(d)}$ and dispersion surface; $\overline{XX'} = 2q$.
$\overline{WW'} = 2q \cos(\theta_B - \theta_0) = \overline{XX'} \cos(\theta_B - \theta_0)$.
WM, perpendicular distance of W from $S_0^{(d)}$ plane; $\overline{WM} = p$.

Notation:

Wave vectors *in vacuo*.

incident: $\mathbf{K} = \overrightarrow{EO}$;
transmitted primary: $\mathbf{K}_0 = \overrightarrow{EO}$;
transmitted reflected: $\mathbf{K}_g = \overrightarrow{AG}$.

Wave vectors in crystal:

primary: $\mathbf{k}_0^{(1)} = \overrightarrow{A^{(1)}O}$, $\mathbf{k}_0^{(2)} = \overrightarrow{A^{(2)}O}$;
reflected: $\mathbf{k}_g^{(1)} = \overrightarrow{A^{(1)}G}$, $\mathbf{k}_g^{(2)} = \overrightarrow{A^{(2)}G}$.

Mean wave vectors in crystal:

primary: $\mathbf{k}_0 = \overrightarrow{\bar{A}O}$;
reflected: $\mathbf{k}_g = \overrightarrow{\bar{A}G}$.

Resonance errors:

$\overrightarrow{A^{(2)}A^{(1)}} = 2\mathbf{d}$, $\overrightarrow{A_0A^{(1)}} = \mathbf{d}_1$, $\overrightarrow{A_0A^{(2)}} = \mathbf{d}_2$, $\overrightarrow{A_0A_g} = 2\mathbf{t}$.

Positive sense of the direction is taken as the direction toward the origin.

By considering the magnitudes κ_0, κ_g, $\mathbf{k}_0$, $\mathbf{k}_g$ and the lattice potential, we obtained the dispersion surface (equi-energy surface) for an energy E,

$$(\kappa_0-\mathbf{k}_0)\,(\kappa_g-\mathbf{k}_g) = |U_g|^2/4\kappa^2, \tag{7}$$

where

$$\kappa^2 = (2me/h^2)\,(E+V_0) = \mathbf{K}^2+U_0. \tag{8}$$

This gives a hyperbolic surface close to a Bragg reflexion as shown in figure 2. If a wave point is given on the dispersion surface, the wave vectors and the ratio of amplitude of primary and reflected waves are determined. From equation (6), the ratio of amplitudes is given by

$$C = \psi_g/\psi_0 = 2\kappa_0(\kappa_0-\mathbf{k}_0)/-U_{-g} = -U_g/2\kappa_g(\kappa_g-\mathbf{k}_g). \tag{9}$$

The symbols are listed in the legend of figure 2.

The wave points and corresponding wave vectors in the crystal for a given wave vector $\mathbf{K}$ *in vacuo* are determined by the requirement of tangential continuity of wave vectors on the crystal surface as indicated in figure 2. Then it is seen that a pair of waves corresponding to the two branches of the dispersion surface appear in the crystal for the primary and reflected waves respectively. They are expressed by

$$\left.\begin{aligned}\psi_0^{(1)}(\mathbf{r}) &= \psi_0^{(1)}\exp 2\pi i(\mathbf{k}_0^{(1)}\cdot\mathbf{r}),\\ \psi_0^{(2)}(\mathbf{r}) &= \psi_0^{(2)}\exp 2\pi i(\mathbf{k}_0^{(2)}\cdot\mathbf{r}),\end{aligned}\right\} \quad \text{(primary waves)}, \tag{10a}$$

$$\left.\begin{aligned}\psi_g^{(1)}(\mathbf{r}) &= \psi_g^{(1)}\exp 2\pi i(\mathbf{k}_g^{(1)}\cdot\mathbf{r}),\\ \psi_g^{(2)}(\mathbf{r}) &= \psi_g^{(2)}\exp 2\pi i(\mathbf{k}_g^{(2)}\cdot\mathbf{r}),\end{aligned}\right\} \quad \text{(reflected waves)}. \tag{10b}$$

The wave points of primary and reflected waves *in vacuo* outside of the b surface (exit surface) are also determined by a similar requirement and the wave functions of the transmitted waves can be expressed by

$$\Phi_0(\mathbf{r}) = \Phi_0\exp 2\pi i(\mathbf{K}_0\cdot\mathbf{r}), \tag{11a}$$

$$\Phi_g(\mathbf{r}) = \Phi_g\exp 2\pi i(\mathbf{K}_g\cdot\mathbf{r}). \tag{11b}$$

The amplitudes $\psi_0^{(i)}$, $\psi_g^{(i)}$, Φ_0 and Φ_g are determined in terms of Ψ by the boundary conditions on the planes a and b expressed as

$$\Phi(\mathbf{r}_s) = \psi(\mathbf{r}_s), \tag{12a}$$

$$\frac{\partial}{\partial n}\Phi(\mathbf{r}_s) = \frac{\partial}{\partial n}\psi(\mathbf{r}_s), \tag{12b}$$

where $\Phi(\mathbf{r}_s)$ and $\psi(\mathbf{r}_s)$ are wave functions on both sides of the boundary surfaces, $\mathbf{r}_s$ the position vector indicating a point on the surface. Equation (12a) can be satisfied only when the components of K_0, $k_0^{(i)}$, $k_g^{(i)}$ tangential to the surface are equal. It is usual in transmission electron microscopy that the normal components of all wave vectors are large compared with the difference among themselves, because the waves enter the crystal nearly normally. In such a case, these two conditions are approximately equivalent.

Thus the boundary conditions on both boundary surfaces are expressed as

$$\left.\begin{aligned}\sum_{i=1,2}\psi_0^{(i)}(\mathbf{r}_a) &= \Psi(\mathbf{r}_a),\\ \sum_{i=1,2}\psi_g^{(i)}(\mathbf{r}_a) &= 0,\end{aligned}\right\} \quad \text{(on the } a\text{-plane)}, \tag{13}$$

$$\left.\begin{aligned}\Phi_0(\mathbf{r}_b) &= \sum_{i=1,2}\psi_0^{(i)}(\mathbf{r}_b),\\ \Phi_g(\mathbf{r}_b) &= \sum_{i=1,2}\psi_g^{(i)}(\mathbf{r}_b),\end{aligned}\right\} \quad \text{(on the } b\text{-plane)}. \tag{14}$$

PHILOSOPHICAL TRANSACTIONS OF THE ROYAL SOCIETY A MATHEMATICAL, PHYSICAL & ENGINEERING SCIENCES

By inserting (1), (10a) and (10b) into (13), the amplitudes of the crystal waves turn out to be

$$\psi_0^{(i)} = \frac{C^{(1)}C^{(2)}}{C^{(1)}-C^{(2)}}\frac{(-1)^i}{C^{(i)}}\Psi \exp 2\pi i(\mathbf{K}-\mathbf{k}_0^{(i)}\cdot\mathbf{R}_a), \tag{15a}$$

$$\psi_g^{(i)} = C^{(i)}\psi_0^{(i)}. \tag{15b}$$

where $(-1)^i$ means (-1) and (1) for $i=1$ and $i=2$ respectively, and $\mathbf{R}_a$ means the special case of $\mathbf{r}_a$ when it is normal to the entrance surface.

Similarly, by substituting (10a), (10b), (11a), (11b), (15a) and (15b) into (14), the amplitudes of transmitted waves turn out to be

$$\Phi_0 = \frac{C^{(1)}C^{(2)}}{C^{(1)}-C^{(2)}}\Psi \sum_{i=1,2}\frac{(-1)^i}{C^{(i)}} \exp 2\pi i(\mathbf{K}-\mathbf{k}_0^{(i)}\cdot\mathbf{R}_a) \exp 2\pi i(\mathbf{k}_0^{(i)}-\mathbf{K}_0\cdot\mathbf{R}_b), \tag{16a}$$

$$\Phi_g = \frac{C^{(1)}C^{(2)}}{C^{(1)}-C^{(2)}}\Psi \sum_{i=1,2}(-1)^i \exp 2\pi i(\mathbf{K}-\mathbf{k}_0^{(i)}\cdot\mathbf{R}_a) \exp 2\pi i(\mathbf{k}_g^{(i)}-\mathbf{K}_g\cdot\mathbf{R}_b), \tag{16b}$$

where $\mathbf{R}_b$ has the same meaning as $\mathbf{R}_a$ corresponding to the exit surface.

Since the object of this section is to obtain theoretically the wave function of a well-focused transmission electron microscopic image, it is sufficient to evaluate the wave function $\Phi(\mathbf{r})$ at point $\mathbf{r}_b$ on the exit surface of the crystal. $\Phi(\mathbf{r}_b)$ is written from equations (16a), (16b) and (9) as follows:

$$\begin{aligned}
\Phi(\mathbf{r}_b) &= \Phi_0(\mathbf{r}_b)+\Phi_g(\mathbf{r}_b)\\
&= \frac{-C^{(2)}}{C^{(1)}-C^{(2)}}\Psi \exp 2\pi i\{(\mathbf{K}-\mathbf{k}_0^{(1)}\cdot\mathbf{R}_a)+(\mathbf{k}_0^{(1)}-\mathbf{K}_0\cdot\mathbf{R}_b)+\mathbf{K}_0\cdot\mathbf{r}_b\}\\
&\quad+\frac{C^{(1)}}{C^{(1)}-C^{(2)}}\Psi \exp 2\pi i\{(\mathbf{K}-\mathbf{k}_0^{(2)}\cdot\mathbf{R}_a)+(\mathbf{k}_0^{(2)}-\mathbf{K}_0\cdot\mathbf{R}_b)+\mathbf{K}_0\cdot\mathbf{r}_b\}\\
&\quad+\frac{-C^{(1)}C^{(2)}}{C^{(1)}-C^{(2)}}\Psi \exp 2\pi i\{(\mathbf{K}-\mathbf{k}_0^{(1)}\cdot\mathbf{R}_a)+(\mathbf{k}_g^{(1)}-\mathbf{K}_g\cdot\mathbf{R}_b)+\mathbf{K}_g\cdot\mathbf{r}_b\}\\
&\quad+\frac{C^{(1)}C^{(2)}}{C^{(1)}-C^{(2)}}\Psi \exp 2\pi i\{(\mathbf{K}-\mathbf{k}_0^{(2)}\cdot\mathbf{R}_a)+(\mathbf{k}_g^{(2)}-\mathbf{K}_g\cdot\mathbf{R}_b)+\mathbf{K}_g\cdot\mathbf{r}_b\}.
\end{aligned} \tag{17}$$

The deviation from the Bragg angle is expressed by a parameter named the resonance error. This parameter is introduced here by the quantity

$$\overrightarrow{A_0A_g} = 2\mathbf{t} \quad \text{or} \quad \overrightarrow{A^{(2)}A^{(1)}} = 2\mathbf{d}, \tag{18}$$

as indicated in figure 2. At the Bragg angle, they become

$$t = 0 \quad \text{and} \quad d = q. \tag{19}$$

From the relation of a hyperbola and its asymptote, it is seen that

$$-d_1d_2 = q^2 \tag{20}$$

$$d = \sqrt{(t^2+q^2)}. \tag{21}$$

Then

$$\mathbf{d}_1-\mathbf{d}_2 = 2\mathbf{d}, \tag{22}$$

$$\mathbf{d}_1+\mathbf{d}_2 = 2\mathbf{t}. \tag{23}$$

From equations (7), (20) and figure 2, it is seen that

$$q = |U_g|/2\kappa\sqrt{(\cos\theta_0\cos\theta_g)} = p/\sqrt{(\cos\theta_0\cos\theta_g)}. \tag{24}$$

As the Fourier coefficient of lattice potential V_g is given by

$$V_g = \frac{h^2}{2me} U_g,$$

p is given as

$$p = V_g/2\lambda E. \tag{25}$$

In terms of $\theta_{\Delta 0}$, which is an angle of deviation from the Bragg angle, the resonance error is written as (Hashimoto 1954)

$$2t = \kappa\theta_{\Delta 0} \sin 2\theta_B/\cos\theta_g. \tag{26}$$

The ratio of amplitude shown in equation (9), then, is expressed in terms of the parameter $\mathbf{d}$, from the geometry of dispersion surface, as follows:

$$C^{(1)} = -d_1 \cos\theta_0/p, \quad C^{(2)} = -d_2 \cos\theta_0/p. \tag{27}$$

It is convenient at this stage to introduce the mean value of wave vectors in the crystal. In figure 2, $\bar{A}$ represents a wave point with the mean value for the crystal waves.

From the geometry indicated in figure 2, it is seen that

$$\mathbf{k}_0^{(i)} = \mathbf{k}_0 + (-1)^i \mathbf{d}, \tag{28}$$

$$\mathbf{k}_g^{(i)} = \mathbf{k}_g + (-1)^i \mathbf{d}, \tag{29}$$

$$\mathbf{K} = \mathbf{K}_0, \tag{30}$$

$$\mathbf{K}_g = \mathbf{K}_0 + \mathbf{g} - 2\mathbf{t}, \tag{31}$$

where $\mathbf{k}_0$ and $\mathbf{k}_g$ are the mean values for the crystal waves.

Using the values of $C^{(i)}$, $\mathbf{k}_0^{(i)}$ and $\mathbf{k}_g^{(i)}$ given in (27), (28) and (29), we rewrite (17) as

$$\begin{aligned}\Phi(\mathbf{r}_b) = {} & \frac{-d_2}{2d} \Psi \exp 2\pi i\{(\mathbf{k}_0 - \mathbf{K}_0)\cdot\mathbf{Z} - \mathbf{d}\cdot\mathbf{Z} + \mathbf{K}_0\cdot\mathbf{r}_b\} \\ & + \frac{d_1}{2d} \Psi \exp 2\pi i\{(\mathbf{k}_0 - \mathbf{K}_0)\cdot\mathbf{Z} + \mathbf{d}\cdot\mathbf{Z} + \mathbf{K}_0\cdot\mathbf{r}_b\} \\ & - \frac{p}{2d\cos\theta_g} \Psi \exp 2\pi i\{(\mathbf{k}_0 - \mathbf{K}_0)\cdot\mathbf{Z} - \mathbf{d}\cdot\mathbf{Z} + \mathbf{K}_g\cdot\mathbf{r}_b\} \\ & + \frac{p}{2d\cos\theta_g} \Psi \exp (2\pi i\{\mathbf{k}_0 - \mathbf{K}_0)\cdot\mathbf{Z} + \mathbf{d}\cdot\mathbf{Z} + \mathbf{K}_g\cdot\mathbf{r}_b\}\end{aligned} \tag{32}$$

where $\mathbf{Z} = \mathbf{R}_b - \mathbf{R}_a$; the thickness of the crystal.

3. Intensity profile of the image of a plate-shaped crystal

The current density of electrons is proportional to $\Phi(\mathbf{r})\,\Phi^*(\mathbf{r})\,|\mathbf{K}|\cos\theta_0$ the intensity distribution of electron waves at the exit surface of the crystal expressed as

$$I = \Phi(\mathbf{r}_b)\,\Phi^*(\mathbf{r}_b)\,|\mathbf{K}|\cos\theta_0 = (I_1 + I_2)\,|\Psi|^2\,|\mathbf{K}|\cos\theta_0, \tag{33}$$

where

$$I_1 = 1 - (q^2/d^2)\sin^2 2\pi\mathbf{d}\cdot\mathbf{Z} + (p^2/d^2\cos\theta_g)\sin^2 2\pi\mathbf{d}\cdot\mathbf{Z}, \tag{33a}$$

$$I_2 = B\sin 2\pi(\mathbf{g}\cdot\mathbf{x} + \beta), \tag{33b}$$

$$\beta = (1/2\pi)\sin^{-1}(t\sin^2 2\pi\mathbf{d}\cdot\mathbf{Z}/\sqrt{\{(-\tfrac{1}{2}d)^2\sin^2 4\pi\mathbf{d}\cdot\mathbf{Z} + t^2\sin^4 2\pi\mathbf{d}\cdot\mathbf{Z}\}}), \tag{33c}$$

$$B = 2\sqrt{\{(-\tfrac{1}{2}d)^2 \sin^2 4\pi \mathbf{d}\cdot\mathbf{Z} + t^2 \sin^4 2\pi \mathbf{d}\cdot\mathbf{Z}\}}\,(p/d^2 \cos\theta_g), \tag{33d}$$

$$\mathbf{g}\cdot\mathbf{x} = \mathbf{g}\cdot\mathbf{r}_b, \dagger \tag{33e}$$

and x is the co-ordinate on the b-surface.

The term I_1 represented by (33a) is a uniform intensity corresponding to the background of the image. This is nearly equal to unity and equal to the intensity of the incident beam, because the intensity of the primary wave is expressed as

$$I_p = \Phi_0(\mathbf{r})\,\Phi_0^*(\mathbf{r})\,|\mathbf{K}|\cos\theta_0 = \left\{1 - \frac{q^2}{d^2}\sin^2 2\pi \mathbf{d}\cdot\mathbf{Z}\right\}|\Psi'|^2\,|\mathbf{K}|\cos\theta_0, \tag{34a}$$

which corresponds to the first and second terms, and the intensity of the reflected wave is expressed as

$$I_r = \Phi_g(\mathbf{r})\,\Phi_g^*(\mathbf{r})\,|\mathbf{K}|\cos\theta_g = \{(p^2/d^2\cos\theta_g)\sin^2 2\pi \mathbf{d}\cdot\mathbf{Z}\}\,|\Psi'|^2\,|\mathbf{K}|\cos\theta_g, \tag{34b}$$

which corresponds to the third term in equation (33a).

Equation (33b) gives the periodic intensity in the image. From these equations one can easily understand that the image becomes a set of straight lines which are parallel to the lattice plane concerned and the intensity profile is represented by a sine curve with the spacing of the fringes given by $1/|\mathbf{g}| = a$, where a is the spacing of the lattice planes. The positions of the fringes vary with the value of the phase β, i.e. of the parameter d (or t) and the thickness Z.

At the exact Bragg angle ($t = 0$), β becomes zero; then, the periodic term of the image (33b) is given by, when $\cos\theta_0 = \cos\theta_g = 1$,

$$I_2 = -\sin 4\pi pZ \sin 2\pi \mathbf{g}\cdot\mathbf{x} \equiv -A \sin 2\pi \mathbf{g}\cdot\mathbf{x}, \tag{35}$$

where $A = \sin 4\pi pZ$. Thus the first intensity minimum of the fringes is at the point shifted in the positive direction of x by an amount $\frac{1}{4}a$ from the origin, when A is positive.

It is generally believed that the intensity profile of the electron microscopic image represents the variation of mass-thickness. In the image of a crystal lattice, however, this does not hold any longer. If the structure of the crystal is simple and the origin coincides with the centre of symmetry, the mass thickness in the crystal will certainly have a maximum at the origin, because the lattice points (atoms, ions or molecules) are located generally at the centre of symmetry. Therefore the intensity minimum of the fringe should appear at the origin. But in reality, the intensity minimum shifts by an amount of $\frac{1}{4}a$, i.e. an image of the crystal lattice does not indicate the mass-thickness in the crystal.

As can be seen from equations (33) and (35), the sign of p decides the sign of the amplitude of the fringes when the thickness is constant, i.e. from equation (25) the sign of the Fourier coefficient of inner potential V_g decides the mode of maxima and minima of the fringes. If the sign of V_g is negative, the intensity minimum of the predicted fringes changes to a maximum. If the crystal has no centre of symmetry, V_g is expressed as $|V_g|\ \mathrm{e}^{-\mathrm{i}\varphi}$, where φ is the phase angle of the crystal. In such a case, equations (33b) and (33c) are written as

$$I_2 = B\sin\{2\pi(\mathbf{g}\cdot\mathbf{x} + \beta) - \varphi\}, \tag{36}$$

$$B = 2\sqrt{\{(-\tfrac{1}{2}d)^2 \sin^2 4\pi \mathbf{d}\cdot\mathbf{Z} + t^2 \sin^4 2\pi \mathbf{d}\cdot\mathbf{Z}\}}\,(|p|/d^2\cos\theta_g). \tag{36a}$$

The fringes, therefore, are shifted by an amount $a\varphi/2\pi$.

† In equation (33), $(\mathbf{g} - 2\mathbf{t})\cdot\mathbf{r}_b$ is replaced by $\mathbf{g}\cdot\mathbf{r}_b$, because $2\mathbf{t}$ is normal to the crystal surface and the fringes are on the exit surface of the crystal.

Figure 3 shows how this function varies with d (or t) and dZ in the range $-\frac{1}{2} \leqslant gx \leqslant \frac{1}{2}$, i.e. $\frac{1}{2}a \leqslant x \leqslant \frac{1}{2}a$. This function is periodic in dZ and gx with period $\frac{1}{2}$ and 1 respectively. The full and dotted curves refer to t positive and negative respectively.

The intensity profile of the fringes of a plate-shaped crystal is given by the condition $Z = C$, where C is constant. In the diagram of the co-ordinates d against dZ, a line of $Z = C$ passes through the origin $d = 0$ as shown in figure 4. Then the fringes of a plate-shaped crystal with various thicknesses and in various conditions are easily obtained from the curves shown in figure 3.

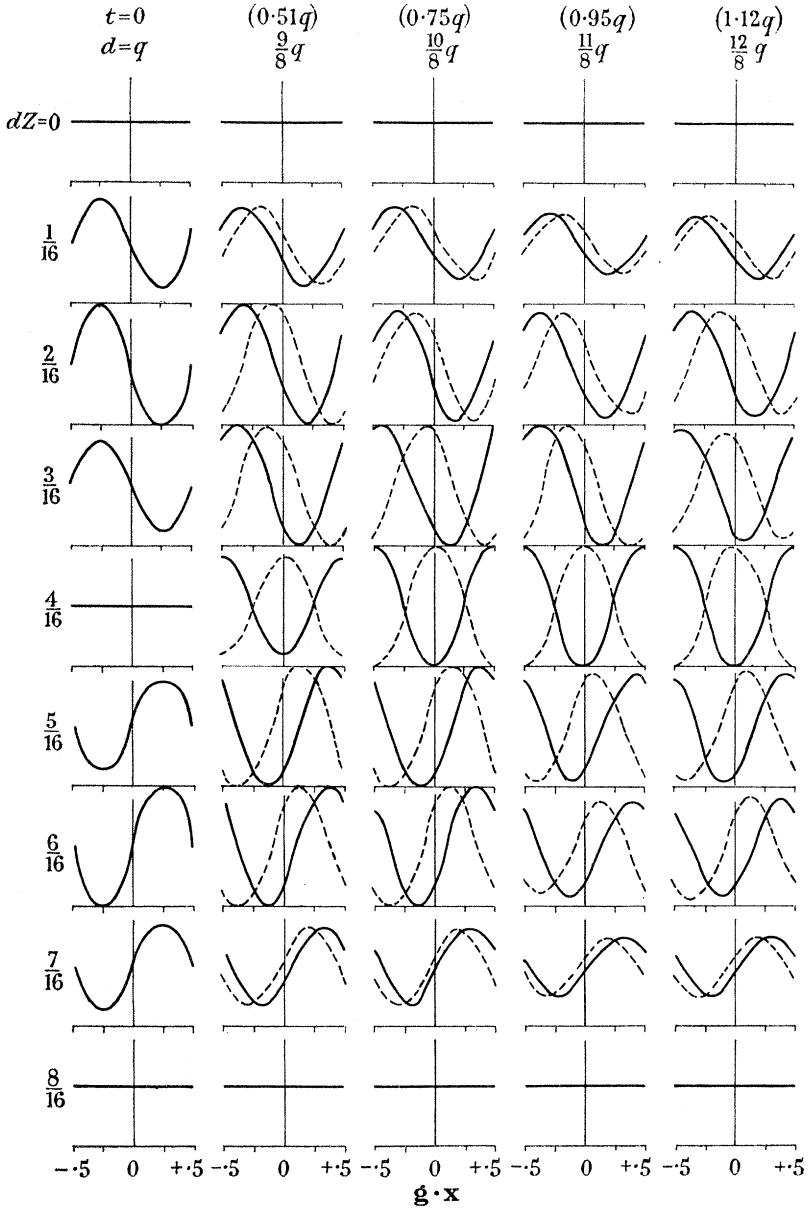

FIGURE 3. The theoretical intensity profile I of the crystal lattice fringes as a function of $\mathbf{g}\cdot\mathbf{x}$. The different curves correspond to various values of d (or t) and dZ. At $d = q$, i.e. at the Bragg-reflecting position, it is clearly seen that the intensity maxima shift by half the fringe spacing wherever the thickness becomes $n/4q$. For $d \neq q$, i.e. for the position deviated from the Bragg angle, intensity maxima shift gradually with increasing thickness and wherever the thickness becomes $n/2q$, the intensity maxima shift by half the fringe spacing.

At the Bragg angle, the profiles of the fringes are given by those on the co-ordinate $d = q$, $(t = 0)$, in figures 3 and 4. The intensity and position of the fringes change with thickness. The variation of the fringes is schematically indicated in figure 5.

As can be seen in figure 5, wherever the thickness becomes $Z = n/4q$ where $n = 1, 2, 3, \ldots$, the fringe has a stepped structure with a shift of half the spacing. The value $1/4q$ is equivalent to half the period of the beat of intensity of primary and reflected waves, i.e. as can be seen from the equations $(34b)$ and $(34a)$, the nodes of the reflected wave will appear at $Z = 1/2q, 2/2q, \ldots$. As the fringe in the image is formed by the interference of primary and reflected waves, it is probable that the fringe disappears at the nodes of primary and reflected waves and has maximum intensity at the thickness where the intensity of primary and reflected waves are the same.

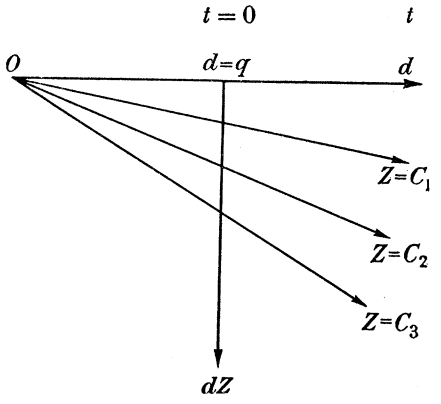

FIGURE 4. Reference diagram of figure 3, showing the lines of $Z = C$ in the co-ordinate d against dZ.

For a deviation from the Bragg angle, the profiles of the fringes are given by those on the co-ordinates $d \neq q$, $(t \neq 0)$, in figures 3 and 4. The profile and position of the fringes vary both with the degree of deviation from the Bragg angle and with increase of thickness. In figure 6, the variation of the fringe due to the increase of thickness is schematically indicated for the cases of $t = 0{\cdot}1q$, $t = 0{\cdot}5q$ and $t = q$.

As can be seen in figure 6, at large deviations from the Bragg angle the fringes shift gradually as the thickness increases and moreover the steps at the thickness $1/4d$, which appeared in figure 5, disappear. In this case, the steps of half the fringe spacing appeared wherever the thickness became $n/2d$, where $n = 1, 2, 3, \ldots$.

The fringes of a bent plate-shaped crystal are formed on extinction contour bands. Along the middle line of an extinction contour band the Bragg condition is exactly satisfied and near the edge of the contour the Bragg condition is not exactly satisfied. Therefore, the variation of the fringes due to the deviation from the Bragg angle will also appear on an extinction contour band. If a crystal is bent into the form of a cylinder of radius R as shown in figure 7, at the point A, the Bragg condition is exactly satisfied and at the point B, located a distance S from the point A, the Bragg condition is not exactly satisfied. The angular deviation $\theta_{\Delta 0}$ of the incident beam at the point B from that corresponding to the exact Bragg condition is equal to the angle of bending α of the crystal. From equation (26),

$$\frac{S}{R} = \alpha \equiv \theta_{\Delta 0} = \frac{\cos\theta_g}{\kappa \sin 2\theta_B} . 2t. \qquad (37)$$

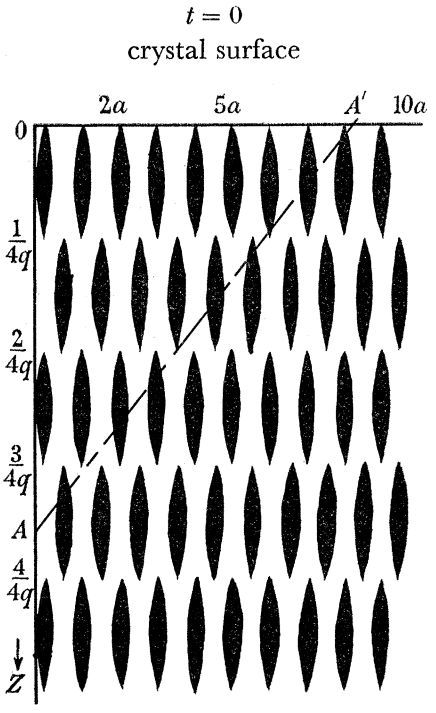

FIGURE 5. Schematic diagram obtained by a study of figure 4, showing the variation of the fringes with varying thickness at the Bragg reflexion position. The dark strips in the figure represent the positions of the minima and their intensity distribution.

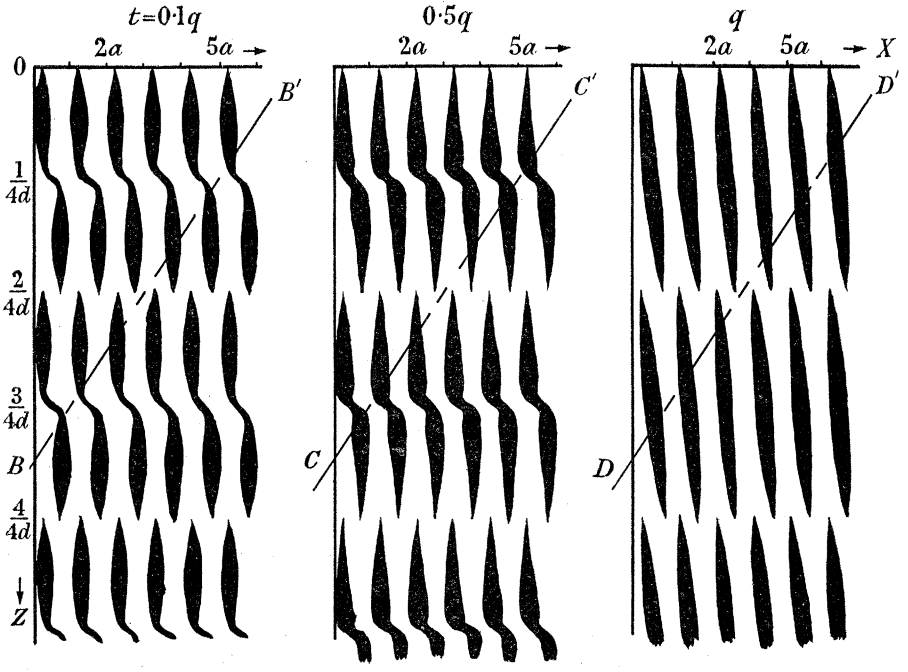

FIGURE 6. Schematic diagram obtained by a study of figures 3 and 4, showing the variation of the fringe with varying thickness for a deviation from the Bragg reflexion positions, (*a*) $t = 0{\cdot}1q$, (*b*) $t = 0{\cdot}5q$, (*c*) $t = q$. The strips represent minima in the intensity profile, $d = \sqrt{(t^2 + q^2)}$.

Therefore, the distance S is proportional to the parameter t, the deviation from the Bragg angle. As the fringe profiles of the bent crystal of uniform thickness are indicated by those on a line of $Z = C$ in the diagram shown in figures 3 and 4, the variation of the fringes on an extinction contour band can easily be seen. In figure 8, fringes of a bent crystal whose mode of bending is as shown in figure 7, i.e. convex to incident beam, on an extinction contour band and its subsidiary are schematically illustrated for four different thicknesses.

The lines represent minima in the intensity profile and the thickness of the lines represents the intensity of the lines. The equally spaced thin lines whose spacing is the same as that of the original lattice represent the positions of the same kinds of centre of symmetry in the crystal, one of which is adopted as the origin in the present consideration. As was stated above, in the crystal with a very simple structure, lattice points are located generally at the centres of symmetry. Then if the electron microscopic image of a crystal lattice represented the mass thickness in the crystal, the fringes would appear exactly on the thin lines.

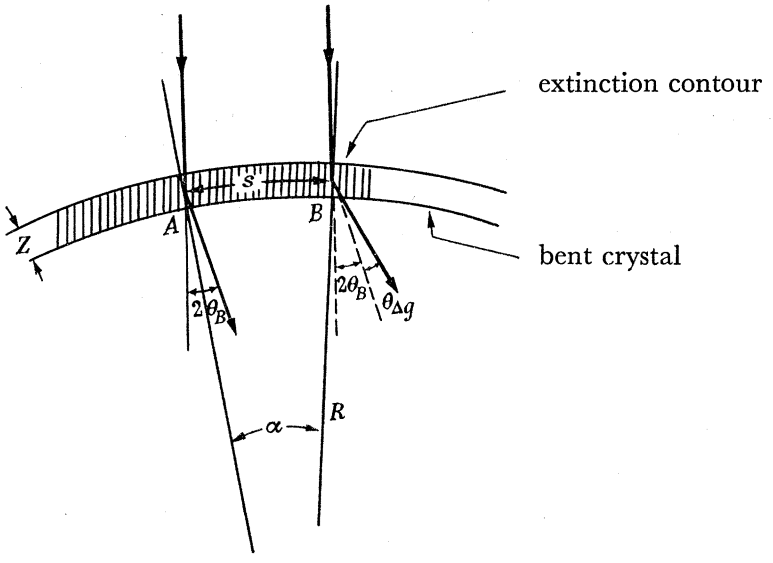

FIGURE 7. Cross-section of a crystal bent into a form of cylinder of radius R indicating the relation of the Bragg reflexion and the extinction contour band.

As can be seen in this diagram, at the thickness of $1/8q$, which corresponds to about 300 Å for the image of the $(20\bar{1})$ plane of Pt-phthalocyanine, the fringe along the middle line of the extinction contour band indicates the same spacing as that of the original lattice and has maximum contrast, but near the edge of the contour the fringes have greater spacing and smaller contrast. The shift of the lines due to the increased separation is half the spacing near the edges of the contour. On the subsidiary extinction contour band, the spacing of the fringes is larger than that of the original lattice and the positions of the lines shift by an amount equal to half the spacing on both edges of the contour.

At the thickness $2/8q$, fringes do not appear along the middle line of the extinction contour and the fringes near the edge of the contour have increased spacing. At the thickness $3/8q$, the contrast of the fringes at the middle of the contour is the reverse of that for the thickness $1/8q$, i.e. the positions of the lines shift by half the fringe spacing, and near the edge of the contour the separation of the fringes is increased rather than decreased. At the

thickness $4/8q$, the fringes do not appear along the middle line of the contour and have increased spacing near the edge of the contour. The variation of the fringes on the subsidiary contour for each thickness is nearly the same as for the thickness $1/8q$.

The variation of the fringes between the thickness 0 and $1/2q$ described above is repeated for thicknesses between $1/2q$ and $1/q$, if the absorption is neglected. In general, the spacing of the fringes near the edge of the contour is larger than that near the middle line and the intensity of the fringes near the edge is less than that near the middle line.

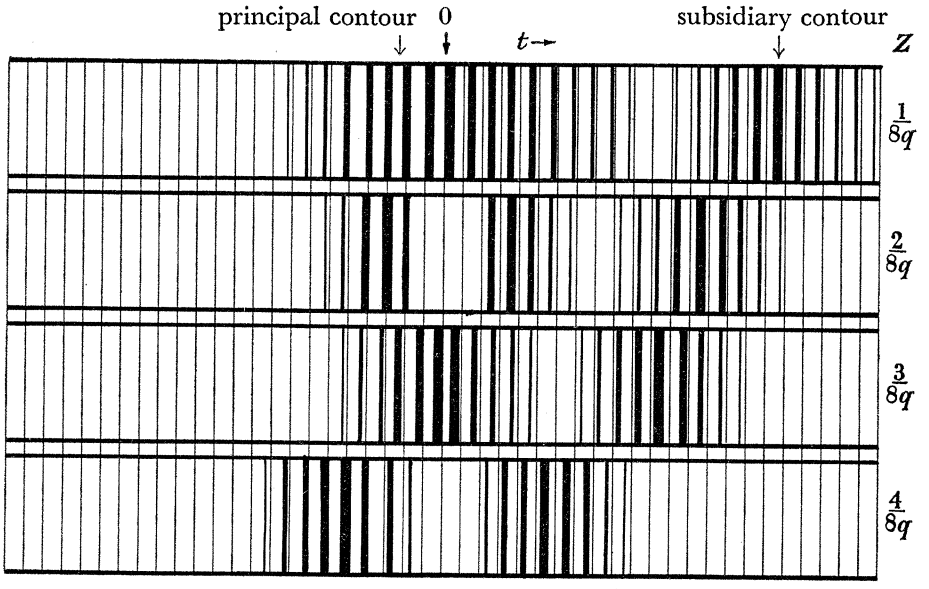

FIGURE 8. Schematic diagram obtained by a study of figures 4, 5 and 6, showing the change of appearance of the fringes of a bent crystal with a mode of bending as shown in figure 7, as the thickness is varied. The lines represent the positions of minima in the intensity profile and the thickness of the lines represent the intensity of the profile. The equally spaced thin lines represent the positions of the centres of symmetry in the crystal, where mass-thickness in the crystal shows certain maxima or minima in a simple crystal. Thickness $1/8q$ corresponds to 300 Å for $(20\bar{1})$ plane of Pt-phthalocyanine.

4. WAVE FUNCTION AND INTENSITY PROFILE OF THE IMAGE OF A WEDGE-SHAPED CRYSTAL

The image of a crystal lattice which seems to have a thickness anomaly has often been observed in electron microscopic images. In this section the image of such a crystal is treated.

Let us assume here, for simplicity, that the crystal is wedge-shaped with two flat surfaces not parallel to each other and that both areas are large enough for the effect of the edge to be neglected, i.e. the tangential continuity of wave vectors holds approximately. The incident wave is assumed to be nearly normal to only one surface, the entrance surface (a), and waves in the crystal are assumed to leave only from another surface, the exit surface (b). It is further assumed that the wave vectors of the beams are nearly normal to the boundary surfaces so that the normal components of all wave vectors are large compared with differences among themselves.

Under these assumptions, as was suggested by Kato (1952), crystal waves can be determined by the entrance surface independent of the exit surface and the transmitted waves which are connected with the crystal waves are determined only by the exit surface.

In order to interpret the various kinds of lattice image of a wedge-shaped crystal it is sufficient to interpret the following two kinds of lattice image. One is an image of lattice planes parallel to the edge of the wedge (yz plane shown in figure 9 (a)) and the other is an image of lattice planes perpendicular to the edge of the wedge (xz plane shown in figure 9 (b)).

In the case shown in figure 9 (a), the preceding interpretation of the image of a plate-shaped crystal is not applicable, because the exit surface is not parallel to the entrance surface. However, as stated above, the transmitted waves which are connected with the crystal waves can be determined by the exit surface only.

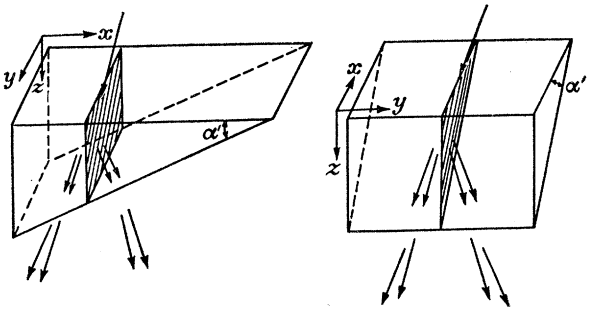

FIGURE 9. Two kinds of lattice plane in a wedge-shaped crystal and the waves in the crystal and *in vacuo*. If rectangular co-ordinates are taken as follows, x and y are normal and parallel directions to the edge of wedge respectively and z is normal to xy plane, two kinds of lattice plane are indicated by yz plane and xz plane as indicated by shading in (a) and (b) respectively.

The wave points of the transmitted waves are determined on the dispersion surface shown in figure 10 by the condition of tangential continuity. As the normals n_a and n_b are not parallel to each other, the two wave points, $B^{(1)}$ and $B^{(2)}$, or transmitted primary waves, do not coincide with that of the incident wave E, and they are separated from each other. Similarly, those of the reflected waves, $C^{(1)}$ and $C^{(2)}$ are also separated.

By using the wave vectors given in figure 10, the wave functions of the transmitted wave are written as follows,

$$\Phi(\mathbf{r}) = \Phi_0(\mathbf{r}) + \Phi_g(\mathbf{r}) = \sum_{i=1,2} \Phi_0^{(i)}(\mathbf{r}) + \sum_{i=1,2} \Phi_g^{(i)}(\mathbf{r}), \tag{38}$$

$$\Phi_0^{(i)}(\mathbf{r}) = \Phi_0^{(i)} \exp 2\pi i(\mathbf{K}_0^{(i)} \cdot \mathbf{r}), \tag{38a}$$

$$\Phi_g^{(i)}(\mathbf{r}) = \Phi_g^{(i)} \exp 2\pi i(\mathbf{K}_g^{(i)} \cdot \mathbf{r}). \tag{38b}$$

The boundary condition on the b plane is as follows:

$$\left.\begin{aligned} \Phi_0^{(i)}(\mathbf{r}_b) &= \psi_0^{(i)}(\mathbf{r}_b), \\ \Phi_g^{(i)}(\mathbf{r}_b) &= \psi_g^{(i)}(\mathbf{r}_b). \end{aligned}\right\} \tag{39}$$

By substituting (9) and (38) into (39), the amplitudes of the transmitted waves become

$$\Phi_0^{(i)} = \frac{C^{(1)}C^{(2)}}{C^{(1)} - C^{(2)}} \frac{(-1)^i}{C^{(i)}} \psi \exp 2\pi i\{(\mathbf{K} - \mathbf{k}_0^{(i)}\mathbf{R}_a) + (\mathbf{k}_0^{(i)} - \mathbf{K}_0^{(i)} \cdot \mathbf{R}_b)\}, \tag{40a}$$

$$\Phi_g^{(i)} = \frac{C^{(1)}C^{(2)}}{C^{(1)} - C^{(2)}} (-1)^i \psi \exp 2\pi i\{(\mathbf{K} - \mathbf{k}_0^{(i)}\mathbf{R}_a) + (\mathbf{k}_g^{(i)} - \mathbf{K}_g^{(i)} \cdot \mathbf{R}_b)\}. \tag{40b}$$

From the geometrical construction shown in figure 10 the following relations are obtained:

$$\mathbf{k}_0^{(i)} = \mathbf{k}_0 + (-1)^i \mathbf{d}, \tag{41a}$$

$$\mathbf{k}_g^{(i)} = \mathbf{k}_0^{(i)} + \mathbf{g}, \tag{41b}$$

$$\mathbf{K}_0^{(i)} = \mathbf{K}_0 + (-1)^i \alpha' d \mathbf{U}_g, \tag{41c}$$

$$\mathbf{K}_g^{(i)} = \mathbf{K}_g + (-1)^i \alpha' d \mathbf{U}_g, \tag{41d}$$

$$\mathbf{K}_g - \mathbf{K}_0 = \mathbf{g} - \mathbf{l}, \tag{42}$$

$$\mathbf{Z} = \mathbf{R}_b - \mathbf{R}_a, \tag{43}$$

$$l = \frac{2t \cos\theta_B}{\cos(\alpha' - \theta_\beta)} - \frac{|\boldsymbol{\kappa} - \mathbf{K}| - t\cos\theta_B}{\cos\theta_B} \sin\alpha' \tan 2\theta_B \doteqdot 2t, \tag{44}$$

where $\mathbf{U}_g$ is a unit vector parallel to $\overrightarrow{GO}$.

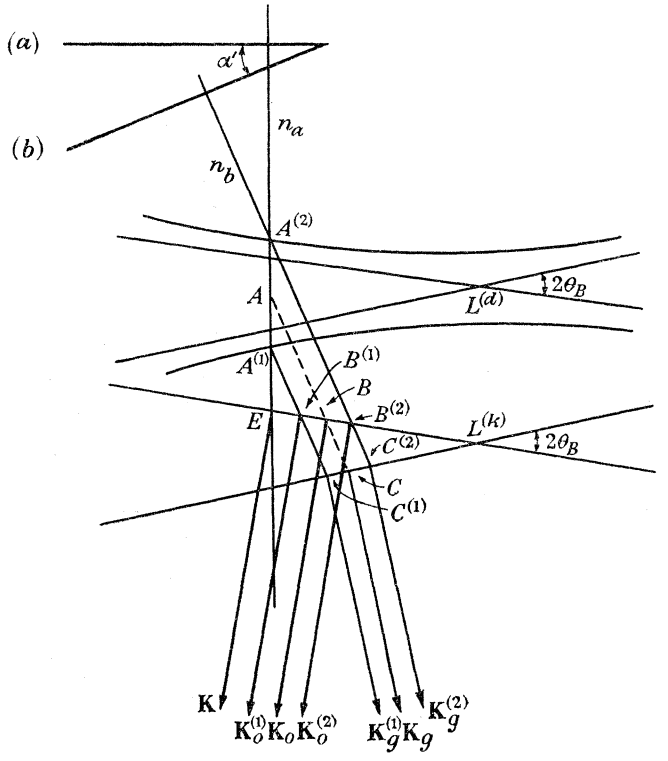

FIGURE 10. Dispersion surface and wave points for a wedge-shaped crystal. A, B and C are the mean wave points of $A^{(1)}$, $B^{(1)}$ and $C^{(1)}$.

$$\overrightarrow{BC} = \mathbf{l}, \quad |\overrightarrow{B^{(2)}B^{(1)}}| \doteqdot |2\alpha d| \doteqdot |\overrightarrow{C^{(2)}C^{(1)}}|, \quad \overrightarrow{EO} = \mathbf{K}, \quad \overrightarrow{B^{(1)}O} = \mathbf{K}_0^{(1)},$$
$$\overrightarrow{B^{(2)}O} = \mathbf{K}_0^{(2)}, \quad \overrightarrow{BO} = \mathbf{K}_0, \quad \overrightarrow{C^{(1)}G} = \mathbf{K}_g^{(1)}, \quad \overrightarrow{CG} = \mathbf{K}_g, \quad \overrightarrow{C^{(2)}G} = \mathbf{K}_g^{(2)}.$$

Then, the wave function of the transmitted wave (34) is rewritten as follows:

$$\begin{aligned}\Phi(\mathbf{r}) = \frac{\Psi}{2d} &\exp 2\pi i\{\mathbf{K}\cdot\mathbf{R}_a + \mathbf{k}_0\cdot\mathbf{Z}\} \\ &\times [\{d_1 \exp 2\pi i(\mathbf{d}\cdot\mathbf{Z} + \alpha' d\mathbf{U}_g\cdot\mathbf{R}) - d_2 \exp 2\pi i(-\mathbf{d}\cdot\mathbf{Z} - \alpha' d\mathbf{U}_g\cdot\mathbf{R})\} \exp 2\pi i\mathbf{K}_0\cdot\mathbf{R} \\ &+ p\{\exp 2\pi i(\mathbf{d}\cdot\mathbf{Z} + \alpha' d\mathbf{U}_g\cdot\mathbf{R}) - \exp 2\pi i(-\mathbf{d}\cdot\mathbf{Z} - \alpha' d\mathbf{U}_g\cdot\mathbf{R})\} \\ &\times \exp 2\pi i(\mathbf{K}_g\cdot\mathbf{R} + \mathbf{g}\cdot\mathbf{R}_b)],\end{aligned} \tag{45}$$

where $$\mathbf{R} = \mathbf{r} - \mathbf{R}_b.$$

In the present case, the focus cannot be adjusted to the whole portion of the exit surface, because the exit surface is not perpendicular to the incident beam. Therefore let us assume that the focus is adjusted to a point c on the exit surface, which is an intersection point of the normal to the exit surface passing through the origin and the surface as shown in figure 11. The interference fringe on the exit surface can be projected to the image plane. Then, by using the relations

$$\mathbf{r} = \mathbf{r}_b = \mathbf{x}+\mathbf{y}+\mathbf{R}_b, \quad |\mathbf{z}| = |\mathbf{Z}|-\alpha' x, \quad \mathbf{g}\cdot\mathbf{y} = \mathbf{g}\cdot\mathbf{R}_b = \alpha' d\mathbf{U}_g\cdot\mathbf{y} = \mathbf{l}\cdot\mathbf{y} = 0, \tag{46}$$

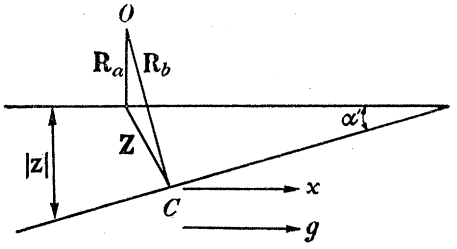

FIGURE 11. Cross-section of a wedge-shaped crystal. O, origin; C, object point to which focus is adjusted, $\mathbf{Z} = \mathbf{R}_b - \mathbf{R}_a$, $|\mathbf{z}| = |\mathbf{Z}| - \alpha' x$.

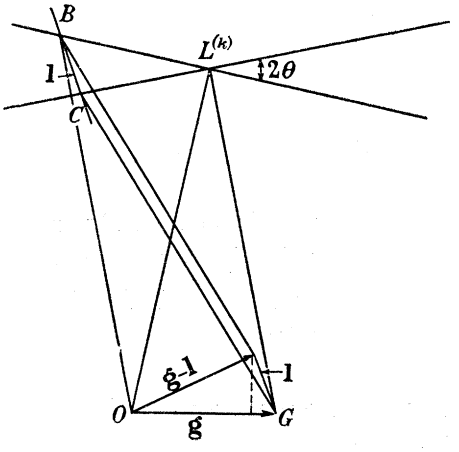

FIGURE 12. Dispersion surface construction, showing the relation between $\mathbf{g}$, $\mathbf{l}$ and $\mathbf{g}-\mathbf{l}$.

we can obtain the following intensity profile corresponding to the image:

$$I = (I_1+I_2)\,|\psi|^2\,|\mathbf{K}|\cos\theta_0, \tag{47}$$

$$I_1 = 1-\frac{q^2}{d^2}\sin^2 2\pi\mathbf{d}\cdot\mathbf{z}+\frac{p^2}{d^2\cos\theta_g}\sin^2 2\pi\mathbf{d}\cdot\mathbf{z}, \tag{47a}$$

$$I_2 = B\sin 2\pi\{(\mathbf{g}-\mathbf{l})\cdot\mathbf{x}+\beta\}, \tag{47b}$$

$$B = 2\sqrt{\{(-\tfrac{1}{2}d)^2\sin^2 4\pi\mathbf{d}\cdot\mathbf{z}+t^2\sin^4 2\pi\mathbf{d}\cdot\mathbf{z}(p/d^2\cos\theta_g)\}}, \tag{47c}$$

$$\beta = (2\pi)^{-1}\sin^{-1}\{t\sin^2 2\pi\mathbf{d}\cdot\mathbf{z}/\sqrt{\{(-\tfrac{1}{2}d)^2\sin^2 4\pi\mathbf{d}\cdot\mathbf{z}+t^2\sin^4 2\pi\mathbf{d}\cdot\mathbf{z}\}}\}, \tag{47d}$$

where $|\mathbf{z}|$ is the local thickness of the crystal corresponding to the predicted fringes.

By comparing equation (47) with equation (33), we can easily understand that the intensity profile of the fringe has a form similar to that for a plate-shaped crystal. In the present case, however, the thickness $|\mathbf{z}|$ varies linearly along the direction normal to the lines

of the fringe. Therefore, both the intensity and the position of the fringes change with the thickness of the crystal. For example, the spacing of the fringes is not given uniquely by the relation from equation (47*b*)

$$(\mathbf{g}-\mathbf{l})\cdot\mathbf{x}_a = 1 \tag{48}$$

because the thickness $|\mathbf{z}|$ in the term β varies with co-ordinate x. By referring to the dispersion surface construction shown in figure 12, we can see that the spacing of the fringes is given in the form,

$$|\mathbf{x}_a|_\beta = 1/\{|\mathbf{g}|-|\mathbf{l}|\,\alpha'+\beta_{\alpha'}\}, \tag{49}$$

where $\beta_{\alpha'}$ is the additional term corresponding to the phase term β, i.e. corresponding to the shift of the fringes due to the deviation from the Bragg angle. At the exact Bragg angle, $t = 0$, the spacing is given by

$$|\mathbf{x}_a| = 1/|\mathbf{g}| = a. \tag{50}$$

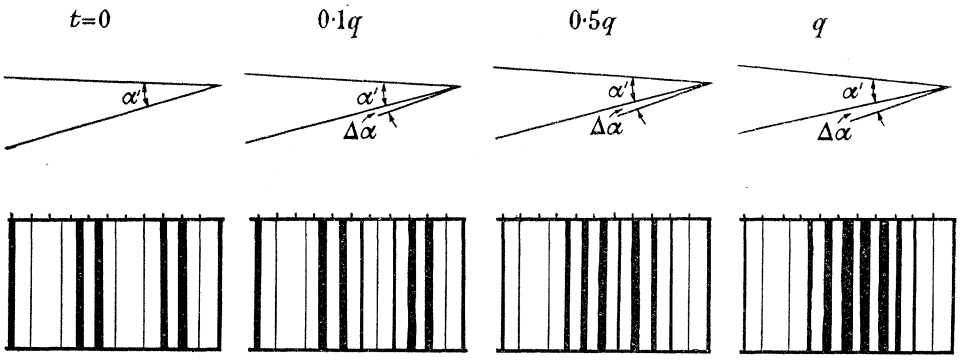

FIGURE 13. Schematic diagrams of the fringes of a wedge-shaped crystal at the Bragg angle (*a*) and at deviated angles (*b*), (*c*), (*d*).

(*a*) $t = 0$; (*b*) $t = 0{\cdot}1q$, corresponding to $\theta_{\Delta 0} = 8{\cdot}6\times10^{-4}$ rad for $(20\bar{1})$ plane of Pt-phthalocyanine; (*c*) $t = 0{\cdot}5q$, $\theta_{\Delta 0} = 4{\cdot}3\times10^{-3}$ rad; (*d*) $t = q$, $\theta_{\Delta 0} = 8{\cdot}6\times10^{-3}$ rad.

The spacing of the scale shown at the upper end of each fringe is different in each case and given by $1/(|\mathbf{g}|-\alpha'|\mathbf{l}|+\beta_{\alpha'}) \doteqdot a/(1-2t\alpha' a)$.

The appearance of the fringes for the wedge-shaped crystal is shown in figures 5 and 6.

At the exact Bragg angle, the fringes are given by the intersection with a line AA' shown in figure 5. The spacing of the lines drawn in the schematic figure 5 should be $1/|\mathbf{g}| = a$ in the present case, according to equation (50). A schematic diagram of the fringes is given in figure 13*a*. The contrast of the fringes reverses always with a thickness increase of $n/4q$ ($n = 1, 2, 3, \ldots$) and so the fringe lines between the thickness $1/4q$ and $1/2q$ are observed as if they shift by an amount of half of the spacing relative to those between 0 and $1/4q$.

At a position deviated from the Bragg angle, the fringes are given by the intersection with the lines BB', CC' and DD' in figures 6 (*a*), (*b*) and (*c*) respectively. The spacings of the lines drawn in the diagrams should not be given in the present case by $1/|\mathbf{g}| = a$ but by $1/\{|\mathbf{g}|-\alpha'\,|\mathbf{l}|+\beta_{\alpha'}\} = a_t$. The schematic diagram of the fringes is illustrated in figures 13 (*b*), (*c*) and (*d*). At the thickness $n/2d$, the fringes fade out, and with increasing thickness, fringes appear again with a shift of $\frac{1}{2}a_t$. The spacings of the fringes vary considerably near the portion where the thickness of the crystal is $n/4d$.

In the case shown in figure 9 (*b*), wave vectors of the primary and reflected waves which leave the crystal are in two planes nearly parallel to the yz plane due to the refraction effect

at the wedge of the crystal. Wave vectors in the crystal and *in vacuo* are determined from the construction of the dispersion surface, as indicated in figure 14. Symbols for wave points, wave vectors, the normal of crystal surfaces and resonance errors are the same as those shown in figure 10.

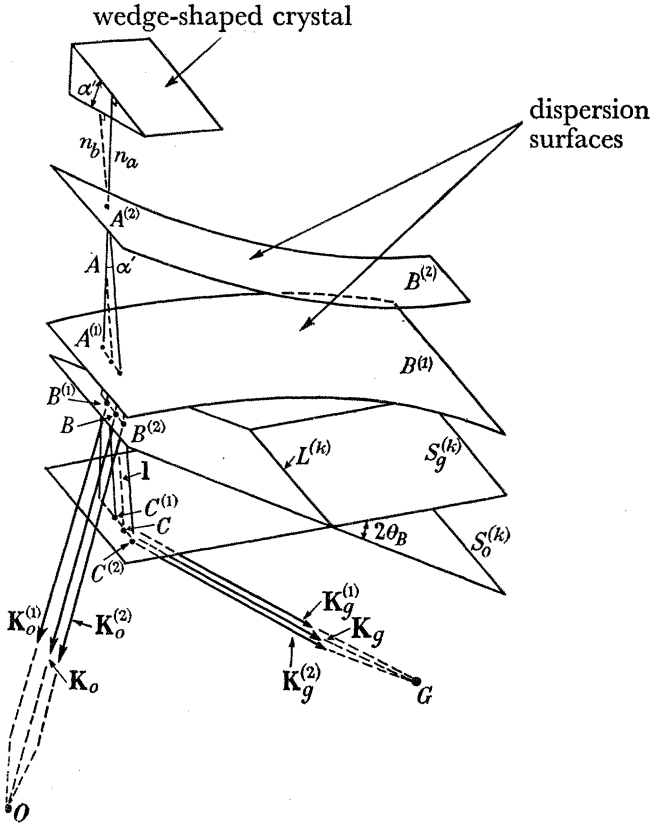

FIGURE 14. Dispersion surface and wave points for the wedge-shaped crystal shown in figure 9 (*b*). Symbols are the same as those shown in figure 10.

By using the same process as in the case shown in figure 9 (*a*), the wave function and corresponding intensities on the exit surface of the crystal can be derived. The intensity profile of the fringe is given by

$$I = (I_1 + I_2)\,|\Psi|^2\,|\mathbf{K}|\cos\theta_0, \tag{51}$$

$$I_1 = 1 - (q^2/d^2)\sin^2 2\pi\mathbf{d}\cdot\mathbf{z} + (p^2/d^2\cos\theta_g)\sin^2 2\pi\mathbf{d}\cdot\mathbf{z}, \tag{51a}$$

$$I_2 = B\sin\{(\mathbf{g}-\mathbf{l})\cdot\mathbf{y}+\beta\}, \tag{51b}$$

$$B = 2\sqrt{\{(-\tfrac{1}{2}d)^2\sin^2 4\pi\mathbf{d}\cdot\mathbf{z} + t^2\sin^4 2\pi\mathbf{d}\cdot\mathbf{z}\}}\,(p/d^2\cos\theta_g), \tag{51c}$$

$$\beta = (2\pi)^{-1}\sin^{-1}[t\sin^2 2\pi\mathbf{d}\cdot\mathbf{z}/\sqrt{\{(-\tfrac{1}{2}d)^2\sin^2 4\pi\mathbf{d}\cdot\mathbf{z} + t^2\sin^4 2\pi\mathbf{d}\cdot\mathbf{z}\}}], \tag{51d}$$

$$|\mathbf{l}| = 2\,|\mathbf{t}|/\cos\alpha'. \tag{51e}$$

By comparing equation (51) with equation (33), it can easily be seen that the intensity profile of the predicted fringes is also given by an equation similar to that for a plate-shaped crystal. Therefore, by studying the intensity profile shown in figures 3, 4, 5 and 6, the fringes corresponding to the lattice image can easily be observed.

In the present case, the thickness $|\mathbf{z}|$ varies linearly along the direction of the x-axis and fringes are formed parallel to the x-axis. The spacing of the fringes is given by

$$(\mathbf{g}-\mathbf{l})\cdot\mathbf{y} = 1. \tag{52}$$

By referring to the dispersion surface construction shown in figure 14, it can be seen that the spacing of the fringes is given by

$$|\mathbf{y}_a| = 1/|\mathbf{g}| = a \tag{53}$$

because $\mathbf{y}\cdot\mathbf{l} = 0$.

In figures 15 (*a*), (*b*), (*c*) and (*d*) the fringes corresponding to the exact Bragg angle and positions deviating from the Bragg angle are indicated. In figure 15 (*a*), the fringes at the Bragg angle are shown and in figure 15 (*b*) the fringes at a deviated position are indicated, with an angle of deviation corresponding to $\Delta\alpha = 8{\cdot}6\times10^{-4}$ rad for the $(20\bar{1})$ plane of Pt-phthalocyanine. (*c*) and (*d*) are those corresponding to $\Delta\alpha = 4{\cdot}3\times10^{-3}$ and $8{\cdot}6\times10^{-3}$ rad for the same plane.

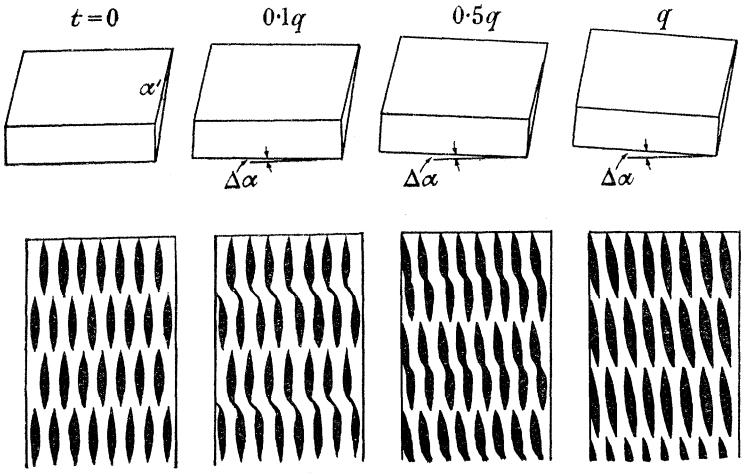

FIGURE 15. Orientations of the wedge-shaped crystal and corresponding lattice fringes. (*a*) at exact Bragg angle; (*b*) at deviated position from Bragg angle. $t = 0{\cdot}1q$ corresponding to $\theta_{\Delta 0} = 8{\cdot}6\times10^{-4}$ rad for $(20\bar{1})$ of Pt-phthalocyanine; (*c*) $t = 0{\cdot}5q$, $\theta_{\Delta 0} = 4{\cdot}3\times10^{-3}$ rad; (*d*) $t = q$, $\theta_{\Delta 0} = 8{\cdot}6\times10^{-3}$ rad.

As can be seen in figure 15, the fringes have a stepped structure with periods given by $(1/4q)\tan\alpha'$ and $(1/2d)\tan\alpha'$ for the situations at the Bragg angle and at deviated angles respectively. In the case of $(20\bar{1})$ plane of Pt-phthalocyanine of wedge angle

$$\alpha' = 14^\circ\,30' = 1/4\,\text{rad},$$

the period $(1/4q)\tan\alpha'$ is 2800 Å.

At the thicker portion of the wedge-shaped crystal, absorption of electrons cannot be neglected. The effect of absorption is presented in the following section.

5. Effect of absorption

The intensities of primary and reflected waves in a crystal are decreased by the inelastic scattering of electrons. The effect of inelastic scattering on electron diffraction by crystals was studied theoretically by Yoshioka (1957). He interpreted the effect on the dynamical theory of electron diffraction and concluded that the absorption coefficients ϵ_i of the two sets of waves $\mathbf{k}_0^{(i)}$, $\mathbf{k}_g^{(i)}$, where $i = 1$ and 2, are different and are given by

$$\epsilon_i = \frac{4\pi me}{h^2\kappa_0}\left\{\frac{-C_{00}}{\cos\theta_0} + \frac{2me}{h^2\kappa_0}\frac{|V_g|\,C_{0g}}{(\xi_i+\eta_i)\cos\theta_0}\right\}, \tag{54}$$

where C_{00} and C_{0g} are the imaginary parts of additional terms to V_0 and V_g respectively and ξ_i, η_i are resonance errors which are given to the first approximation by the relation

$$\xi_i \cdot \eta_i = \left(\frac{me}{h^2 \kappa_0}\right)^2 |V_g|^2. \tag{55}$$

Uyeda (1957) briefly reported that as the thickness of the crystal increases, the contrast and the amount of the steps in the fringes of wedge-shaped crystals as shown in figure 15 will decrease owing to the absorption of electrons.

In this section, the intensity profile of the fringe is discussed with the absorption taken into consideration quantitatively, following Yoshioka.

By using two absorption coefficients given by equation (54), the wave function of the transmitted waves on the exit surface of a plate-shaped crystal is expressed as

$$\begin{aligned}\Phi(\mathbf{r}_b) = {} & (1/2d)\, \Psi' \exp 2\pi i\{(\mathbf{k}_0 - \mathbf{K}_0)\cdot\mathbf{Z} + \mathbf{K}_0\cdot\mathbf{r}\} \\ & \times [\{d_1 \exp(-\tfrac{1}{2}\epsilon_1 Z + 2\pi i\, \mathbf{d}\cdot\mathbf{Z}) - d_2 \exp(-\tfrac{1}{2}\epsilon_2 Z - 2\pi i\, \mathbf{d}\cdot\mathbf{Z})\} \\ & + (p \exp 2\pi i\, \mathbf{g}\cdot\mathbf{r}/\cos\theta_g)\{\exp(-\tfrac{1}{2}\epsilon_1 Z + 2\pi i\, \mathbf{d}\cdot\mathbf{z}) - \exp(-\tfrac{1}{2}\epsilon_2 Z - 2\pi i\, \mathbf{d}\cdot\mathbf{Z})\}].\end{aligned} \tag{56}$$

Then the corresponding intensity profile of the fringes will be given by

$$I_{\text{obs.}} = \Phi(\mathbf{r}_b)\, \Phi^*(\mathbf{r}_b)\, |\mathbf{K}| \cos\theta_0 = I \cdot |\Psi'|^2\, |\mathbf{K}| \cos\theta_0, \tag{57}$$

$$\begin{aligned} I = {} & \frac{1}{4d^2}[\{d_1 \exp(-\tfrac{1}{2}\epsilon_1 Z) - d_2 \exp(-\tfrac{1}{2}\epsilon_2 Z)\}^2 - 4q^2 \exp\{-\tfrac{1}{2}(\epsilon_1 + \epsilon_2) Z\} \sin^2 2\pi\, \mathbf{d}\cdot\mathbf{Z}] \\ & + \frac{p^2}{4d^2 \cos^2\theta_g}[\{\exp(-\tfrac{1}{2}\epsilon_1 Z) - \exp(-\tfrac{1}{2}\epsilon_2 Z)\}^2 + 4 \sin^2 2\pi\, \mathbf{d}\cdot\mathbf{Z} \exp\{-\tfrac{1}{2}(\epsilon_1 + \epsilon_2) Z\}] \\ & - \frac{p}{d\cos\theta_g} \exp\{-\tfrac{1}{2}(\epsilon_1 + \epsilon_2) Z\} \sin 4\pi\, \mathbf{d}\cdot\mathbf{Z} \sin 2\pi\, \mathbf{g}\cdot\mathbf{r}_b \\ & + \frac{p}{2d^2 \cos\theta_g}[\{d_1 \exp(-\epsilon_1 Z) + d_2 \exp(-\epsilon_2 Z)\} - 2t \exp\{-\tfrac{1}{2}(\epsilon_1 + \epsilon_2) Z\} \\ & \times \cos 4\pi\, \mathbf{d}\cdot\mathbf{Z}] \cos 2\pi\, \mathbf{g}\cdot\mathbf{r}_b. \end{aligned} \tag{57a}$$

The first two terms indicate the intensity of the background of the fringes and the third and fourth terms represent the periodic terms of the fringes. As can be seen from equation (57), with increasing thickness of the crystal, the intensity of the background and the contrast of the fringes decrease and moreover the position of the fringes will be shifted.

At the exact Bragg angle ($t = 0$, $d = q$), the intensity profile of the fringes turns out to be

$$\begin{aligned} I = {} & \tfrac{1}{4}\{\exp(-\tfrac{1}{2}\epsilon_1 Z) + \exp(-\tfrac{1}{2}\epsilon_2 Z)\}^2 + \tfrac{1}{4}\{\exp(-\tfrac{1}{2}\epsilon_1 Z) - \exp(-\tfrac{1}{2}\epsilon_2 Z)\}^2 \\ & - \exp(-\{\tfrac{1}{2}(\epsilon_1 + \epsilon_2) Z\} \sin 4\pi\, \mathbf{d}\cdot\mathbf{Z} \sin 2\pi\, \mathbf{g}\cdot\mathbf{r}_b \\ & + \tfrac{1}{2}\{\exp(-\epsilon_1 Z) - \exp(-\epsilon_2 Z)\} \cos 2\pi\, \mathbf{g}\cdot\mathbf{r}_b, \end{aligned} \tag{58}$$

where $\cos\theta_0 = \cos\theta_g = 1$. By comparing with equation (33), it can be seen that the contrast of the fringes is decreased by the coefficients of absorption and the position of the fringes shifts by the effect of the fourth term and, moreover, at $\mathrm{d}Z = n/2$ the fringe does not disappear but shows minimum contrast.

Intensity profiles of the fringes due to the variation of thickness were numerically calculated for the case of an MgO crystal. By referring to the values calculated by Yoshioka

and the intensity anomaly of doubly refracted waves observed by Honjo & Mihama (1954), the values of C_{00} and C_{0g} were estimated to be $C_{00} = -1{\cdot}5\,\mathrm{V}$, and $C_{0g} = 0{\cdot}3\,\mathrm{V}$. Then, for example, at the exact Bragg angle $\epsilon_1 = 1{\cdot}9 \times 10^5\,\mathrm{cm}^{-1}$ and $\epsilon_2 = 2{\cdot}9 \times 10^5\,\mathrm{cm}^{-1}$ were obtained. In figure 16, the intensity profiles are schematically illustrated for various thicknesses, where dotted curves represent those of negative value of t. From equation (58), it can be seen that the thickness which gives one-tenth intensity of the incident wave is about 950 Å. As the values of $V_{(200)}$ and $V_{(220)}$ are calculated as 7·8 V and 5·4 V respectively, 950 Å corresponds to $dZ = 4{\cdot}4/4$ and $3{\cdot}1/4$ for (200) and (220) planes respectively. By referring to these values, two kinds of fringes which are expected to be observed at the wedge of an MgO crystal are indicated in figure 17. As can be seen from figure 17, the variation of the fringes due to the variation of thickness is similar to that with no absorption. However,

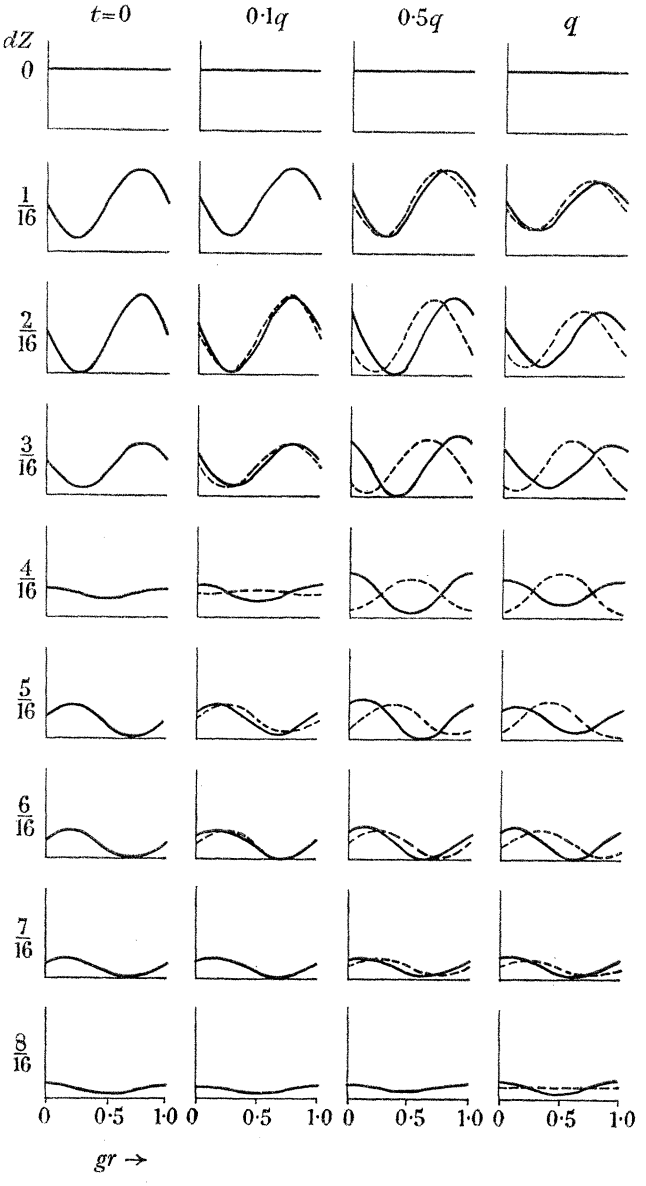

FIGURE 16. Intensity profiles of the fringe of an MgO crystal suffering from absorption for various thicknesses and deviations from the Bragg angle. Dotted curves represent those for negative values of t. $V_g = 4\,\mathrm{V}$, $E = 80\,\mathrm{kV}$ (cf. figure 3).

the intensity of the background and the contrast of the fringes are decreased and, moreover, the amount of the shift of the fringes at the thickness $n/4p$ is not $\frac{1}{2}a$ but becomes smaller as the thickness increases.

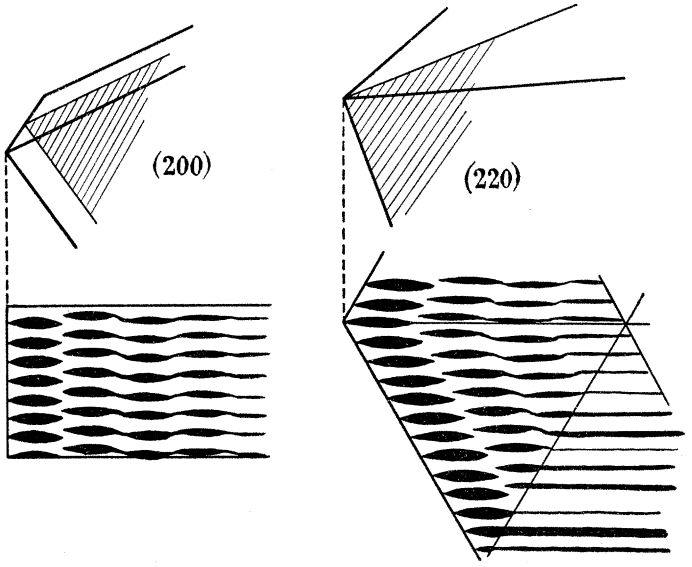

FIGURE 17. Two kinds of wedges of an MgO crystal, and the corresponding fringes which are formed by the reflexion from (200) and (220) planes ($t = 0$).

6. EFFECT OF DIVERGENCE OF THE ILLUMINATION

In an ordinary electron microscope, the illumination is not perfectly axial but has a small angular divergence. In this section, the effect of divergent illumination on the contrast of the image at exact focus is discussed using the dynamical theory of electron diffraction.

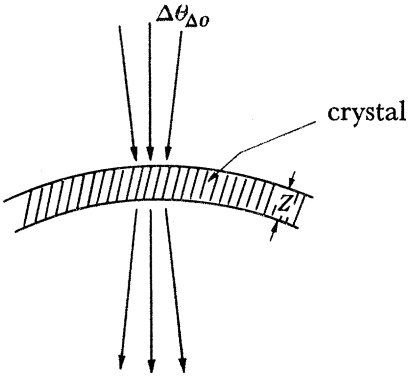

FIGURE 18. Divergent beam whose semi-angle of divergence is $\Delta\theta_{\Delta 0}$ irradiates a crystal of thickness Z.

Let us assume that the divergent beam whose semi-angle of divergence is $\Delta\theta_{\Delta 0}$ irradiates a crystal as shown in figure 18. If the axial beam enters the crystal with a resonance error t (or d) to a lattice plane of the crystal, a beam which is inclined to the axis with an angle $\Delta\theta_{\Delta 0}$ will enter the crystal with a resonance error $(t + \Delta t)$ to the same lattice plane, where Δt is a resonance error corresponding to the angle $\Delta\theta_{\Delta 0}$ and the relation is given by equation (26), i.e.

$$\Delta t = G . \Delta\theta_{\Delta 0}, \tag{59}$$

where $G = \kappa \sin 2\theta_B / 2 \cos\theta_g$.

The intensity profile of the fringes of the crystal lattice illuminated by the divergent beam may be expressed, by assuming $\Delta\theta_{\Delta 0}$ is very small ($\simeq 10^{-2} \sim 10^{-3}$ rad),

$$I(t+\Delta t) = I(\theta_{\Delta 0}+\Delta\theta_{\Delta 0}) = \int_{\theta_{\Delta 0}-\Delta\theta_{\Delta 0}}^{\theta_{\Delta 0}+\Delta\theta_{\Delta 0}} I(\theta_{\Delta 0})\,\mathrm{d}\theta_{\Delta 0}/2\Delta\theta_{\Delta 0} = I(\theta_{\Delta 0}) + \tfrac{1}{6}I''(\theta_{\Delta 0})\,(\Delta\theta_{\Delta 0})^2 + \cdots, \tag{60}$$

where $I(\theta_{\Delta 0})$ is equal to I of equation (33) and $I(\theta'')$ is given by

$$\begin{aligned} I''(\theta) = {} & \frac{pG^2 \sin 2\pi\mathbf{g}\cdot\mathbf{x}}{d^5 \cos\theta_g}\left[(d^2 - 3G^2\theta^2 + 16\pi^2 Z^2 d^2\theta^2 G^2)\sin 4\pi\mathbf{d}\cdot\mathbf{Z}\right. \\ & \left. + 4\pi\mathbf{d}\cdot\mathbf{Z}(3G^2\theta^2 - d^2)\cos 4\pi\mathbf{d}\cdot\mathbf{Z}\right] \\ & + \frac{2pG\theta\cos 2\pi\mathbf{g}\cdot\mathbf{x}}{d^6\cos\theta_g}\left[2G^2(4G^2\theta^2 - d^2)\sin^2 2\pi\mathbf{d}\cdot\mathbf{Z}\right. \\ & \left. + 2\pi\mathbf{d}\cdot\mathbf{Z}G^2(3d^2 - 5G^2\theta^2)\sin 4\pi\mathbf{d}\cdot\mathbf{Z} + 8\pi^2 Z^2 G^4\theta^2\cos 4\pi\mathbf{d}\cdot\mathbf{Z}\right]. \end{aligned} \tag{61}$$

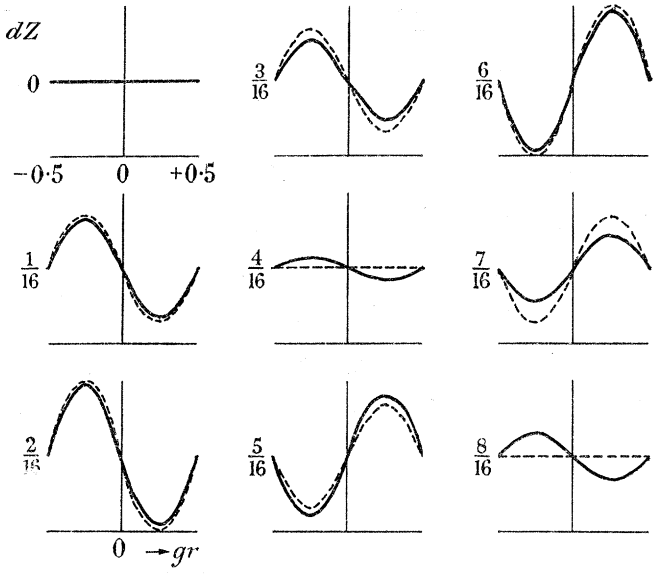

FIGURE 19. Intensity profile of the fringes of a crystal at the exact Bragg angle illuminated by a divergent beam of $\Delta\theta_{\Delta 0} = 5\times 10^{-3}$ rad for the case of spacing 12 Å and $V_g = 2{\cdot}4$ V which are equivalent to those of $(20\bar{1})$ plane of Pt-phthalocyanine. The dotted line represents the case of a parallel beam.

As can be seen from equation (60), the intensity profile of the fringe varies with the term $\frac{1}{6}I''(\theta_{\Delta 0})\,(\Delta\theta_{\Delta 0})^2$. Consequently, if a crystal which is at a position deviating from the Bragg angle is irradiated by a divergent beam, both the position and the intensity of the fringes change from those of parallel illumination. If the crystal which is at the exact Bragg angle is irradiated by a divergent beam, equation (60) turns out to be

$$I(\pm\Delta\theta_{\Delta 0}) = 1 - \frac{pG^2}{6q^3\cos\theta_g}\left[\left\{\frac{6q^2}{G^2} - (\Delta\theta_{\Delta 0})^2\right\}\sin 4\pi qZ + 4\pi qZ(\Delta\theta_{\Delta 0})^2\cos 4\pi qZ\right]\sin 2\pi\mathbf{g}\cdot\mathbf{x}. \tag{62}$$

In figure 19, intensity profiles of the fringes at the exact Bragg angle for crystals which are illuminated by divergent beams of $\Delta\theta_{\Delta 0} = 5\times 10^{-3}$ rad are indicated. As can be seen from equation (62) and figure 19, the position of fringes does not change but the contrast

of the fringes is decreased and, moreover, the contrast of the fringes does not reverse at the thickness $1/4q$ but reverses at the thickness

$$\frac{1}{4q}-\frac{G^2}{24q^3}(\Delta\theta_{\Delta 0})^2,$$

i.e. the period of half integral value of the extinction distance is decreased by an amount

$$\frac{G^2}{24q^3}(\Delta\theta_{\Delta 0})^2$$

which is, for example, equivalent to 35 Å for Pt-phthalocyanine irradiated with a divergence

$$\Delta\theta_{\Delta 0}=5\times 10^{-3}\,\text{rad}.$$

As can be seen from equation (62), at a certain angle of divergence, the contrast of the fringes becomes zero, i.e. the fringes disappear in the continuous background. This critical angle of divergence ($\Delta\theta_c$) is given by

$$(\Delta\theta_c)^2=6q^2\sin 4\pi qZ/G^2(\sin 4\pi qZ-4\pi qZ\cos 4\pi qZ) \qquad (63)$$

and is tabulated in table 1 for the values of spacing a and thickness Z.

TABLE 1. CRITICAL VALUES OF SEMI-ANGLE OF DIVERGENCE FOR WHICH THE FRINGES ARE NOT OBSERVED

	$a=50$ Å, $V_g=1$ V		$a=12$ Å, $V_g=2{\cdot}4$ V		$a=5$ Å, $V_g=5$ V	
qz	Z (Å)	$\Delta\theta_c$	Z (Å)	$\Delta\theta_c$	Z (Å)	$\Delta\theta_c$
0	0	0	0	0	0	0
$\frac{1}{16}$	390	8×10^{-2}	166	$4{\cdot}6\times10^{-2}$	80	4×10^{-2}
$\frac{2}{16}$	780	$3{\cdot}8\times10^{-2}$	333	$2{\cdot}1\times10^{-2}$	160	$1{\cdot}6\times10^{-2}$
$\frac{3}{16}$	1170	$2{\cdot}1\times10^{-2}$	498	$1{\cdot}2\times10^{-2}$	240	$1{\cdot}0\times10^{-2}$
$\frac{4}{16}$	1560	0	666	0	320	0
$\frac{5}{16}$	1950	—	830	—	400	—
$\frac{6}{16}$	2340	$3{\cdot}7\times10^{-2}$	999	$2{\cdot}1\times10^{-2}$	480	$1{\cdot}6\times10^{-2}$
$\frac{7}{16}$	2730	$1{\cdot}5\times10^{-2}$	1162	$8{\cdot}6\times10^{-3}$	560	$7{\cdot}4\times10^{-3}$
$\frac{8}{16}$	3120	0	1332	0	640	0

At larger angles than those tabulated in table 1, according to equation (62), the fringes will show some contrast. In the ordinary electron microscope, however, the objective lens has certain spherical aberration which is given by $\frac{1}{4}C_s\alpha^3$, where C_s is the aberration coefficient and α is the angle between the axis of the lens and a scattered beam. Calculation suggests that at larger divergences than $\Delta\theta_{\Delta 0}\simeq 10^{-2}$, fringes of spacing 12 Å will lose contrast when imaged by a lens of aberration coefficient $C_s\simeq 0{\cdot}3$ cm. Therefore, in order to obtain fringes with some contrast, the semi-angle of divergence has to be smaller than those in table 1.

7. COMPARISON WITH EXPERIMENT

According to the foregoing interpretation, we should observe the anomalies both in spacing and in contrast of the fringes of plate-shaped and wedge-shaped crystals at the positions deviating from the Bragg angle.

In a bent plate-shaped crystal, the fringes will show the anomalies both in spacing and in contrast at the edges of principal extinction contours and on the subsidiary contours as shown in figure 8.

Figure 20 (*a*), (*b*), plate 5, are the micrographs of Pt-phthalocyanine taken by Menter with 10 and 30μ objective apertures respectively. In figure 20 (*a*), all Bragg reflected waves are excluded from the image except the zero order, so one can observe only the extinction contours at the positions indicated by arrows. Extinction contours consist of parallel lines and so it can be deduced that this film has a small bending around one direction parallel to the extinction contour. The strong contour and the weak contours seem to correspond to the principal and subsidiary maxima of the Bragg reflexion respectively. In figure 20 (*b*), the first order of the $(20\bar{1})$ spectrum of the Bragg reflected waves is included in the image so that the lattice fringe is resolved. Figure 20 (*c*) is an enlargement of the enclosed region in (*b*), which indicates that the lattice fringes are clearly resolved and have a spacing anomaly on the principal contour and subsidiary contours.

In order to show the anomaly in spacing and shift of the fringes, a scale of constant spacing is superposed on the fringes. As can be seen in figure 20 (*c*) about 10 lines near the centre of principal contour coincide with the scale but near the edge of the contour, lines in the fringe do not coincide with the scale. Lines formed on the edge of the subsidiary contour are shifted about half of the spacing relative to those on the edge of the principal contour and have increased spacing.

The appearance of the observed fringes coincides with that of the theoretical ones corresponding to the thickness $1/8q$ shown in figure 8. But in order to compare the observed fringes with the theoretical ones quantitatively, it is necessary to know the thickness of this crystal and the Fourier coefficient of the inner potential. If the subsidiary maxima of electron diffraction were observed in a Kossel–Möllenstedt pattern (Kossel & Möllenstedt 1939) or in a high resolution electron diffraction pattern (Hashimoto 1954; Uyeda *et al.* 1954) the thickness of the film and Fourier coefficient of the inner potential would be determined at the same time. At present, however, we have no such measured values. From the structure of Pt-phthalocyanine obtained by Robertson & Woodward (1940) and the atomic scattering factor for electrons obtained by Ibers (1958), the Fourier coefficient of the inner potential can be calculated as 2·4 V for the $(20\bar{1})$ plane. Then, the value $1/8q$ written in figure 8 corresponds to a thickness 300 Å for the crystal irradiated by 80 kV electrons. In the present case, it seems to be not incompatible with the observed relative darkness of the image of the crystal compared with that of the vacuum to assume that the thickness of the crystal is about 300 Å. Therefore, it may be concluded that the coincidence between theory and observation is satisfactory.

Figure 21 (*a*), plate 6, is a micrograph of Cu-phthalocyanine (Hashimoto & Yotsumoto 1959). In this micrograph, there is a notable intensity anomaly; it is so striking that it seems as if due to the thickness anomaly. Even though it is not clear from the present observation whether the crystal has some anomaly in thickness or not, according to the preceding interpretation, the intensity anomaly is expected to be accompanied by a spacing anomaly if the crystal has a small bending.

In order to check the anomaly in spacing, one part of the micrograph, which is outlined, was enlarged and cut into two parts across the fringes (perpendicular to the lines) and one of them arranged upside down as shown in figure 21 (*b*).

The lines indicated by the arrows coincide with each other on both parts of the micrographs but the lines between the arrows do not. It can be observed that the spacings of the

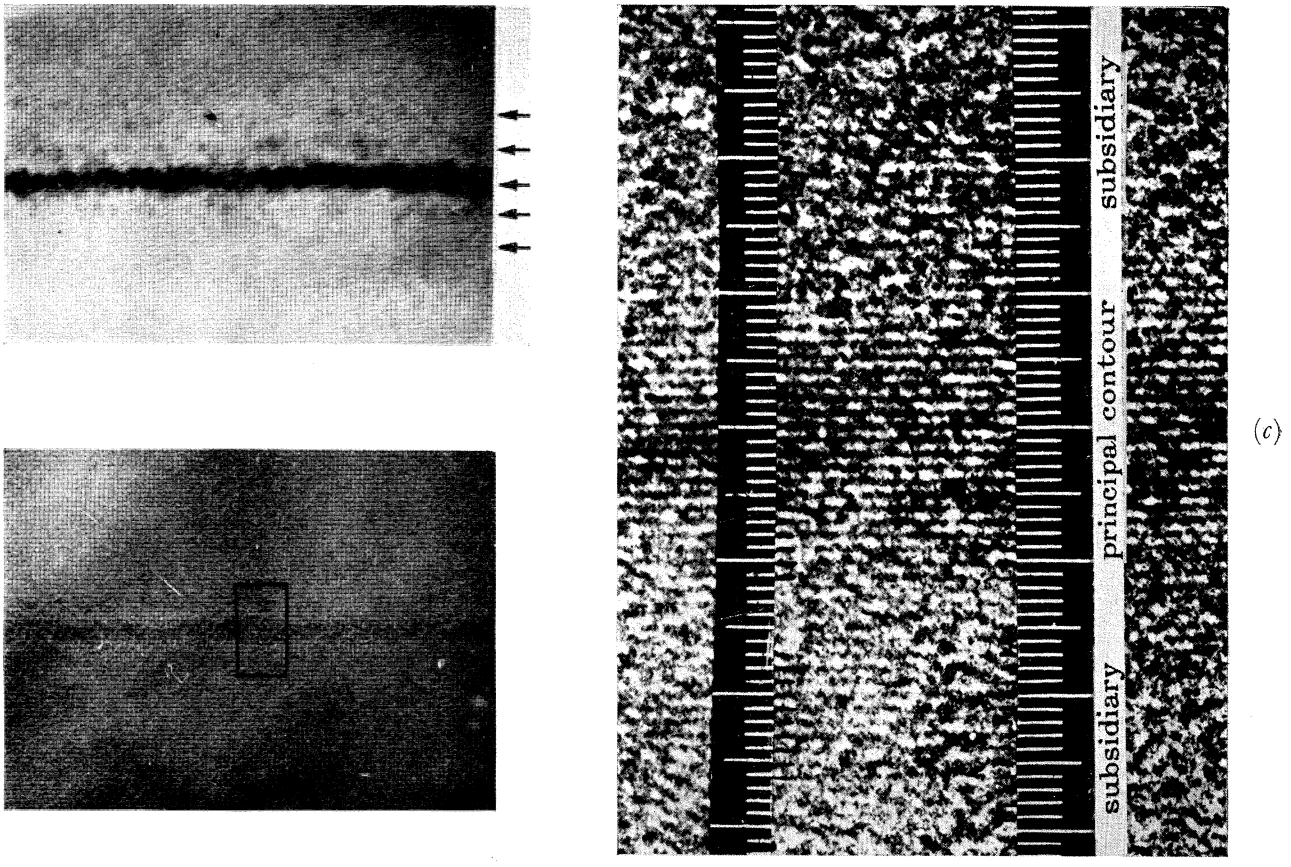

FIGURE 20. (*a*) Principal extinction contour and its subsidiaries in a bent crystal of Pt-phthalocyanine imaged with 10 μ objective aperture so as to pass only the zero-order beam. (Magn. $\times$ 200 000.)

(*b*) Same crystal imaged with 30 μ aperture, showing the fringes of the crystal lattice formed on extinction contours. (Magn. $\times$ 200 000.)

(*c*) Enlargement of enclosed region in (*b*), on which a scale is superposed, showing that the fringes have constant spacing near the centre and increased spacing near the edge of the principal contour, and the fringes on the subsidiary contours have increased spacing (see figure 8). (Magn. $\times$ (1 500 000.) (Courtesy J. W. Menter, 1958, *Phil. Mag. Suppl. Advances in Physics*, **7**, p. 131.)

(*Facing p.* 484)

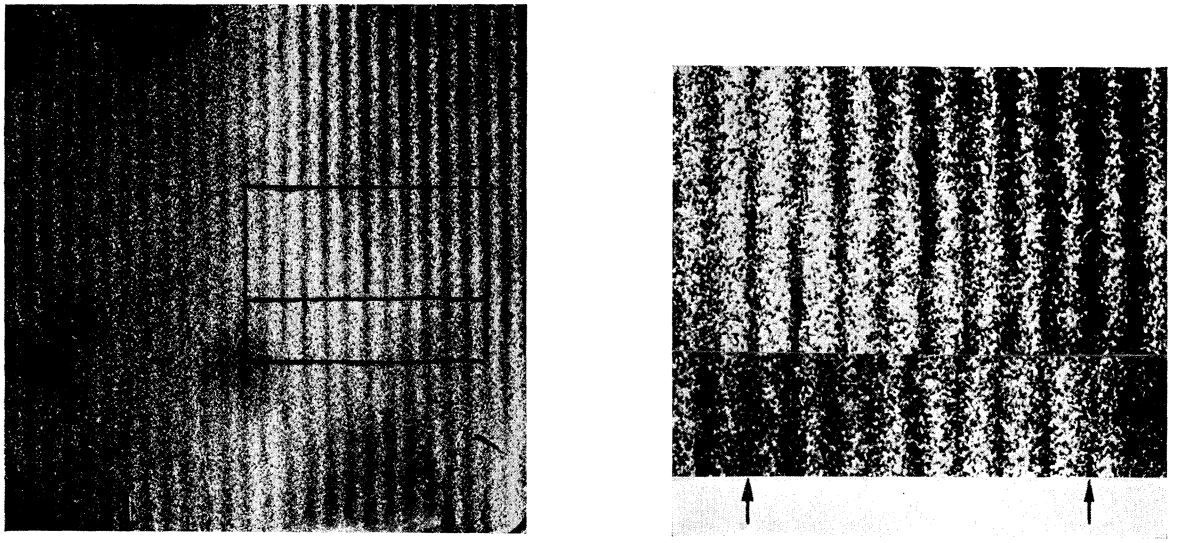

(*a*) (*b*)

FIGURE 21. (*a*) Electron micrograph of Cu-phthalocyanine showing the spacing anomaly of the fringe. Enlargements (*b*) of enclosed regions, one of which is arranged upside down, indicate that the lines between two lines marked by two arrows shift to each other on both parts of the micrograph. (*a*) Magn. × 2 200 000; (*b*) magn. × 5 000 000. (Courtesy *Nature*, 1959, **183**, p. 1001.)

FIGURE 23. Fringe of sodium faujasite showing the stepped structure. By viewing obliquely steps of the fringes are detected along the contours (*a*), (*b*), (*c*), (*d*) and (*e*). (Magn. × 800 000.) (Courtesy J. W. Menter, 1958, *Phil. Mag. Suppl. Advances in Physics*, **7**, p. 132.)

PHILOSOPHICAL TRANSACTIONS OF THE ROYAL SOCIETY A MATHEMATICAL, PHYSICAL & ENGINEERING SCIENCES

weak lines are larger than those of the strong ones. By viewing obliquely along the lines, it can be seen that the amount of shifts between two corresponding lines becomes nearly a quarter of the spacing.

In order to compare the observed spacings with theoretical values quantitatively, it is necessary to know the thickness of this film and the Fourier coefficient of the inner potential. By referring to the structure of Ni-phthalocyanine (Robertson & Woodward 1937), the Fourier coefficient of inner potential of Cu-phthalocyanine was calculated as 3·3 V for the $(20\bar{1})$ plane. Then, the value $1/8p$ written in figure 8 corresponds to 240 Å for the $(20\bar{1})$ plane.

In the present observation, the thickness and the mode of bending cannot be known exactly. The thickness, however, is supposed to be about several hundred ångstroms and the local bending which is always present in a thin plate-shaped crystal is expected to be larger than the angle $\theta = 8 \times 10^{-3}$ rad, which is necessary for the fringe shift of a quarter of the spacing. The present theory, therefore, seems to explain essentially the present observation.

In Zn-phthalocyanine fringes the spacing anomaly and a corresponding intensity anomaly of the fringes, similar to those of Cu-phthalocyanine, were also observed.

In antigorite fringes taken by Yotsumoto (1958), the spacing anomaly was also observed where there was an anomaly of intensity. The region with a spacing anomaly moves as the region with an anomaly of intensity moves, possibly as a result of a buckling of the crystal during the observation. In antigorite, however, the spacing of the fringes is about 90 Å and the thickness of the film is several hundred ångströms. Therefore, the fringes are expected to be formed by the interference of Bragg reflected waves of several orders from the same lattice plane. Then, the spacing anomaly in antigorite fringes may not strictly be interpreted by the present theory. However, it is evident that the wave vectors will change with the deviation from the Bragg angle, and so the shape of the fringes changes with the deviation from the Bragg angle.

In a wedge-shaped crystal, as was stated in the preceding section, there was a periodic reversal of contrast in the fringes. At the exact Bragg angle such a reversal of contrast is at each half integral value of the extinction distance $(1/2q)$ and at a position deviating from the Bragg angle such a reversal occurs at an integral multiple of the extinction distance. If the fringes are not parallel to the apex of the wedge, the fringes are observed to have a stepped structure at the centre and between the extinction contours.

If a wedge-shaped thin crystalline film has some bending and one Bragg reflexion is excited, variation of the fringes due to the thickness anomaly and the deviation from Bragg angle will be observed at the same time. In figure 22, the mode of bending of the crystal and the variation of the fringes are schematically illustrated (absorption of electrons has been taken into account).

Figure 23, plate 6, shows fringes of sodium faujasite taken by Menter. The thickness of the crystal decreases from the lower to the upper side and the fringes are nearly perpendicular to the apex of the wedge. By viewing obliquely, stepped structures (reversal of contrast of the fringes) can be detected along the five contours indicated by arrows (a), (b), (c), (d) and (e). The mode of the stepped structure in the micrograph is quite similar to that of one portion of the illustration shown in figure 22.

PHILOSOPHICAL TRANSACTIONS OF THE ROYAL SOCIETY A MATHEMATICAL, PHYSICAL & ENGINEERING SCIENCES

In order to interpret the appearance of the fringes of sodium faujasite quantitatively, it is necessary to know the angle of wedge (α') and the Fourier coefficient of inner potential V_g of the crystal. At present, we have no method of measuring them. However, if we assume these values as $\alpha' = 0{\cdot}5$ rad $(28^\circ 40')$ and $V_g \simeq 10$ V, the period of the stepped structure becomes 300 Å at the exact Bragg angle and 600 Å at positions deviating from the Bragg angle. The assumed values are seen to be not incompatible with those of sodium faujasite and the calculated period of the stepped structure is nearly equal to the observed value. The fringes formed on the right of this micrograph have steps of shorter period than the ones on the left. This may be due to the larger angle of the wedge of crystal, i.e. the variation of thickness is larger.

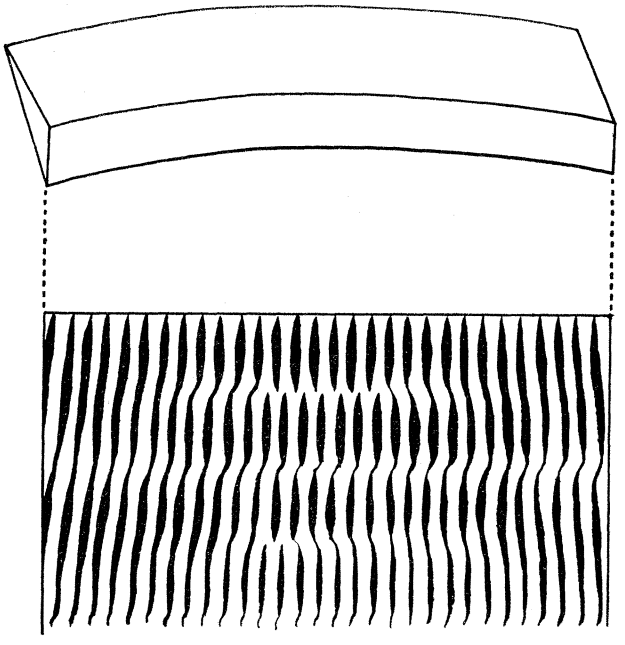

FIGURE 22. A wedge-shaped thin crystalline film with small bending and the corresponding theoretical lattice fringe. (Absorption of electrons has been taken into account.)

Along the contours indicated by arrows (b), (c), (d) and (e), it can really be detected that there are weak traces of the fringes and the intensities of the traces become larger with increasing thickness. The amount of the steps of the fringes becomes less with increasing thickness. By referring to figures 15 (a) and 17, such traces of the fringes along the contours (b), (c), (d) and (e), and the decrease of the relative shift of the steps are seen to be due to the absorption of electrons.

8. CONCLUSION

The present theory has explained the fine structure of the fringes of metal phthalocyanine and sodium faujasite satisfactory and, therefore, it seems to be essentially correct for the interpretation of the fringes of crystal lattices.

The present theory, however, is applicable only to the case of one Bragg reflexion excited in the crystal. In the case where two or more Bragg reflexions are excited from lattice planes of the crystal at the same time, the present theory does not hold any longer. In antigorite fringes, for example, as the spacing is about 90 Å, the fringe is supposed to be formed by the

several waves reflected from a lattice plane simultaneously. In such a case, as was calculated by Heidenreich (1950), Hoerni (1956), Kohra (1954) and Kambe (1957), waves in the crystal will be derived by solving the secular equation of several orders. Even in such a case, if one reflected wave is much stronger than the others, the present theory may be applicable as the first approximation.

Even if the resolving power of transmission electron microscopes is improved very much and reaches, for example, about 0·1 Å, the atomic arrangement in a crystal will still not be revealed in a single image so long as the crystal has a three-dimensional structure. The crystal lattice fringes, as was stated in § 3, do not represent the potential distribution in the crystal. However, if many sets of fringes corresponding to the lattice planes of a crystal are recorded by inclining the illuminating system, it would not be impossible to reveal the atomic arrangement in the crystal such as is shown in a Fourier projection of the inner potential.

As was indicated in § 3, if a crystal is at the exact Bragg angle for a lattice plane g, the intensity profile of the fringe is given, from equations (33), (35), (36), (36a), and (25), as

$$I = 1 - \sin\left\{\frac{2\pi}{\lambda E} Z\,|V_g|\right\} \sin\,(2\pi \mathbf{g}\cdot\mathbf{r} - \varphi), \tag{64}$$

where $\cos\theta_0 = \cos\theta_g = 1$. It must be noted here that the phase angle φ of the crystal is represented as a shift of the fringe by an amount of $a\varphi/2\pi$ and the amplitude of the fringe is given by the function of both thickness Z and Fourier coefficient of periodic potential V_g of the crystal. If the fringes shift laterally by an amount of $\frac{1}{4}a$ $(= \frac{1}{2}\pi)$, the intensity distribution is given by

$$I = 1 + D_g \cos\,(2\pi \mathbf{g}\cdot\mathbf{r} - \varphi), \tag{65}$$

where

$$D_g = \sin\left\{\frac{2\pi}{\lambda E} Z\,|V_g|\right\}. \tag{66}$$

D_g may be called the dynamical structure amplitude for electrons and, for the crystal with small thickness, may be given by

$$D_g \doteqdot \frac{2\pi}{\lambda E} Z\,|V_g|. \tag{67}$$

If many sets of fringes corresponding to $hk0$ reflexion spots of a thin plate-shaped crystal whose surface is parallel to the xy plane of the crystal are recorded each at the exact Bragg angles by inclining the illuminating system, a two-dimensional projection on the xy plane of the potential distribution in crystal would be obtained as follows: Many sets of fringes corresponding to $hk0$ reflexions are taken under the same experimental conditions, and a corner of the crystal or a heavy atom like platinum deposited on the exit surface of the crystal is recorded at the same time as a reference point to decide the origin. These are superposed successively after being shifted laterally by an amount $\frac{1}{4}a_{hk0}$. The integrated intensity distribution of the fringes formed by the superposition of the n sheets of photographs of the fringes is given by

$$\begin{aligned} P(x,y) &= n + \sum_h \sum_k D_{hk} \cos\{2\pi(hx+ky) - \varphi_{hk}\} \\ &= \frac{1}{A'}\left[nA' + \sum_h \sum_k |V_{hk}| \cos\{2\pi(hx+ky) - \varphi_{hk}\}\right], \end{aligned} \tag{68}$$

where

$$A' = \lambda E/2\pi Z.$$

It can be seen easily from equation (68) that the process of superposition is equivalent to Fourier synthesis.

If the crystal is thick, the approximation of equation (67) holds no longer. In such a case, it is necessary to obtain the corresponding fringes with amplitudes $|V_{hk0}|$ from the observed fringes of amplitude D_{hk0}. The corresponding fringes with amplitudes $|V_{hk0}|$ can easily be obtained by using the equation (66), if the thickness of the crystal is measured, for example, from the spacing of subsidiary maxima of electron diffraction spots. The correction of the amplitude due to the thickness of the crystal may correspond to the process which is utilized in structure analysis by electron diffraction methods for eliminating the so-called dynamic extinction effect.

In the case of a very thick crystal, the effect of absorption of electrons cannot be neglected. Then, in order to obtain corresponding fringes of amplitude $|V_{hk0}|$, the effect of absorption described in § 5 has to be taken into account.

The authors would like to express their sincere thanks to Professor K. Tanaka and Professor R. Uyeda for encouragement and helpful discussion during the course of this work, and to Professor A. H. Cottrell, F.R.S., for his help in facilitating the publication of this paper. We would also like to acknowledge our thanks to Dr J. M. Cowley for his interest and helpful discussions in this work and to Dr J. W. Menter for providing copies of his micrographs.

References

Abbe, E. 1837 *Arch. mikr. Anat.* **9**, 413.
Bassett, G. A. & Menter, J. W. 1957 *Phil. Mag.* **2**, 1482.
Bethe, H. A. 1928 *Ann. Phys., Lpz.*, **87**, 55.
Blackman, M. 1939 *Proc. Roy. Soc.* A, **173**, 68.
Brindley, G. W., Comer, J. J., Uyeda, R. & Zussman, J. 1958 *Acta Cryst.* **11**, 99.
Cowley, J. M. 1959 *Acta Cryst.* (in the Press).
Hashimoto, H. 1954 *J. Phys. Soc. Japan*, **9**, 150.
Hashimoto, H. 1958 *J. Phys. Soc. Japan*, **13**, 534.
Hashimoto, H. & Yotsumoto, H. 1959 *Nature, Lond.* **183**, 1001.
Heidenreich, R. D. 1949 *J. Appl. Phys.* **20**, 993.
Heidenreich, R. D. 1950 *Phys. Rev.* **77**, 271.
Hibi, T., Kambe, K. & Honjo, G. 1955 *J. Phys. Soc. Japan*, **10**, 35.
Hoerni, J. 1956 *Phys. Rev.* **102**, 1530, 1534.
Honjo, G. & Mihama, K. 1954 *J. Phys. Soc. Japan*, **9**, 184.
Ibers, J. A. 1958 *Acta Cryst.* **11**, 178.
Kambe, K. 1957 *J. Phys. Soc. Japan*, **12**, 13, 25.
Kato, N. 1952 *J. Phys. Soc. Japan*, **7**, 397, 406.
Kato, N. 1953 *J. Phys. Soc. Japan*, **8**, 350.
Kohra, K. 1954 *J. Phys. Soc. Japan*, **9**, 690.
Kossel, W. & Möllenstedt, G. 1939 *Ann. Phys., Lpz.*, (5), **36**, 113.
Labaw, L. W. & Wyckoff, R. W. G. 1957 *Proc. Nat. Acad. Sci. Wash.* **43**, 1032.
Lentz, F. & Scheffels, W. 1958 *Z. Naturforschung*, **13***a*, 226.
MacGillavry, C. H. 1940 *Physica*, **7**, 329.
Menter, J. W. 1956*a* *Proc. Roy. Soc.* A, **236**, 119.
Menter, J. W. 1956*b* *Proc. Stockholm Conference of Electron Microscopy*, p. 88.
Neider, R. 1956 *Proc. Stockholm Conference of Electron Microscopy*, p. 93.

PHILOSOPHICAL TRANSACTIONS OF THE ROYAL SOCIETY A MATHEMATICAL, PHYSICAL & ENGINEERING SCIENCES

Niehrs, H. 1954 *Z. Phys.* **138**, 570.
Niehrs, H. 1956 *Optik*, **13**, 399.
Ogawa, S., Watanabe, D., Watanabe, H. & Komoda, T. 1958 *Acta Cryst.* **11**, 872.
Robertson, J. M. & Woodward, I. 1937 *J. Chem. Soc.* p. 219.
Robertson, J. M. & Woodward, I. 1940 *J. Chem. Soc.* p. 36.
Thomson, G. P. & Cochrane, W. 1939 *Theory and practice of electron diffraction*, p. 283. London: Macmillan.
Uyeda, R., Ichinokawa, T. & Fukano, Y. 1954 *Acta Cryst.* **7**, 216.
Uyeda, R. 1955 *J. Phys. Soc. Japan*, **10**, 256.
Uyeda, R. 1957 *Metal Phys.* **3**, 65.
Uyeda, R., Masuda, T., Tochigi, H., Ito, K. & Yotsumoto, H. 1958 *J. Phys. Soc. Japan*, **13**, 461.
Whelan, M. J. & Hirsch, P. B. 1957 *Phil. Mag.* **2**, 1121, 1303.
Yoshioka, H. 1957 *J. Phys. Soc. Japan*, **12**, 618.

PHILOSOPHICAL TRANSACTIONS OF THE ROYAL SOCIETY A MATHEMATICAL, PHYSICAL & ENGINEERING SCIENCES

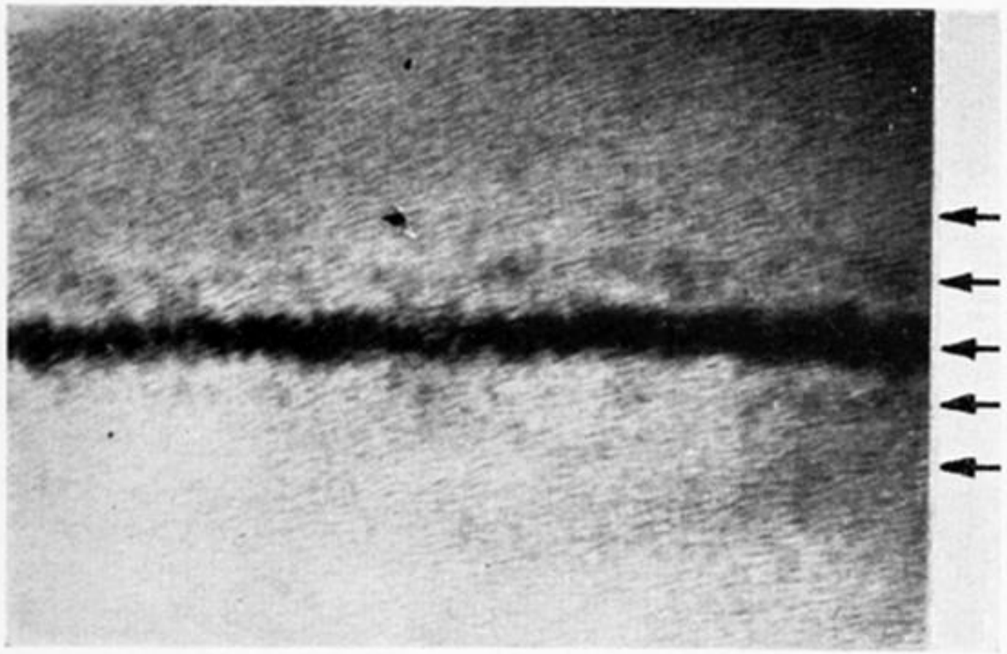

(a)

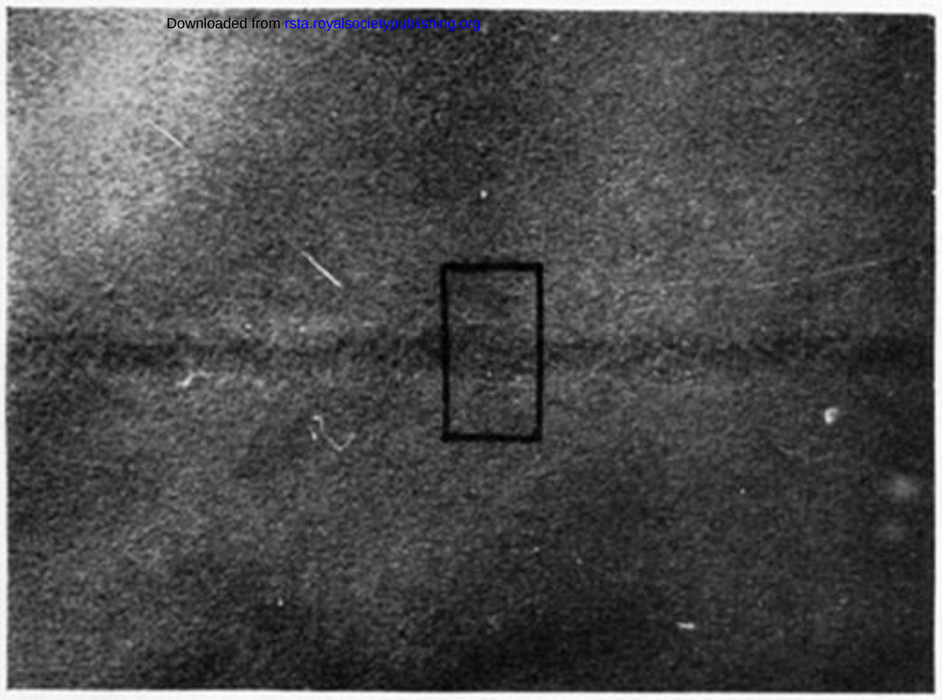

(b)

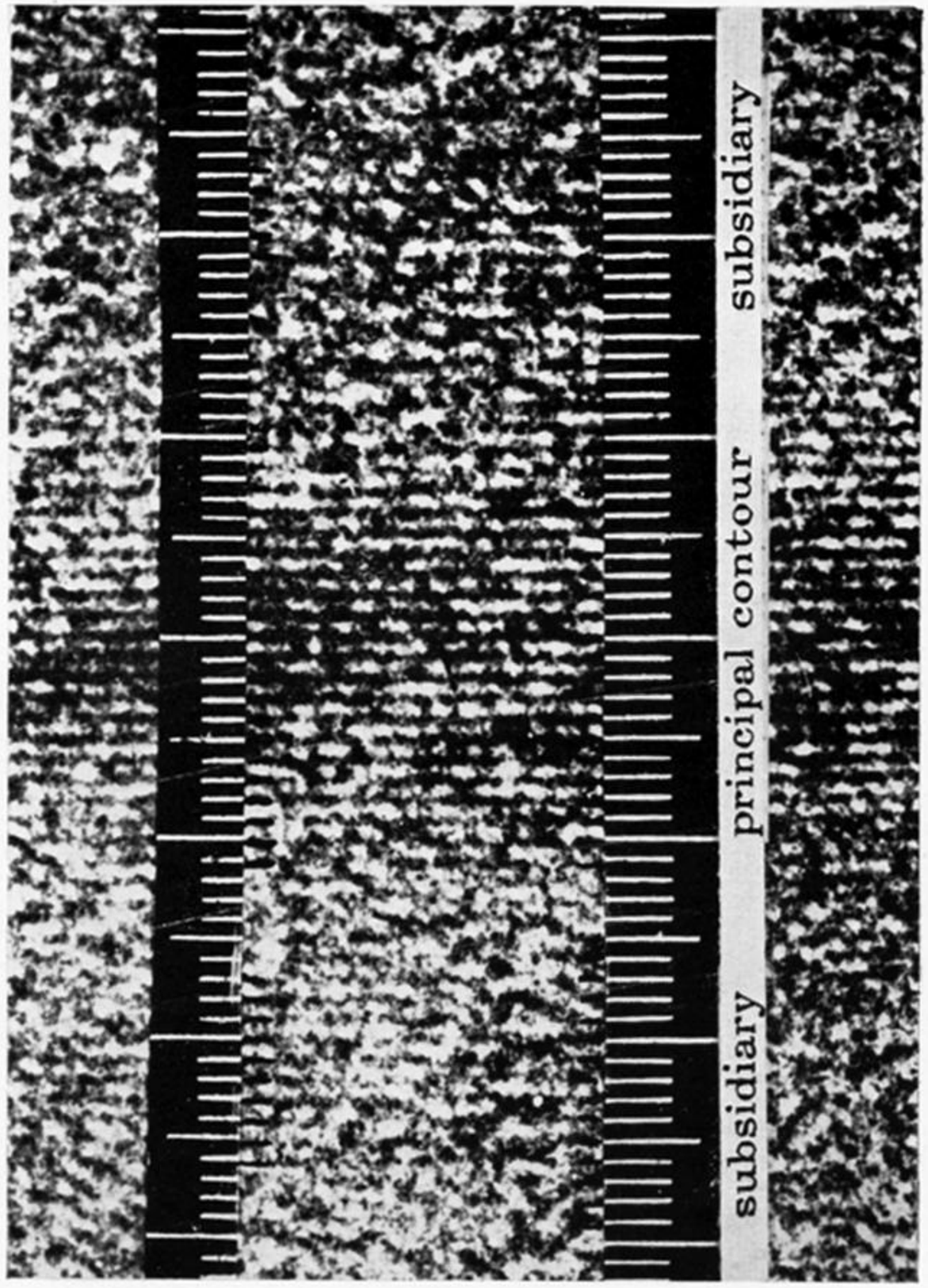

(c)

FIGURE 20. (*a*) Principal extinction contour and its subsidiaries in a bent crystal of Pt-phthalocyanine imaged with 10 μ objective aperture so as to pass only the zero-order beam. (Magn. × 200 000.)

(*b*) Same crystal imaged with 30 μ aperture, showing the fringes of the crystal lattice formed on extinction contours. (Magn. × 200 000.)

(*c*) Enlargement of enclosed region in (*b*), on which a scale is superposed, showing that the fringes have constant spacing near the centre and increased spacing near the edge of the principal contour, and the fringes on the subsidiary contours have increased spacing (see figure 8). (Magn. × (1 500 000.) (Courtesy J. W. Menter, 1958, *Phil. Mag. Suppl. Advances in Physics*, **7**, p. 131.

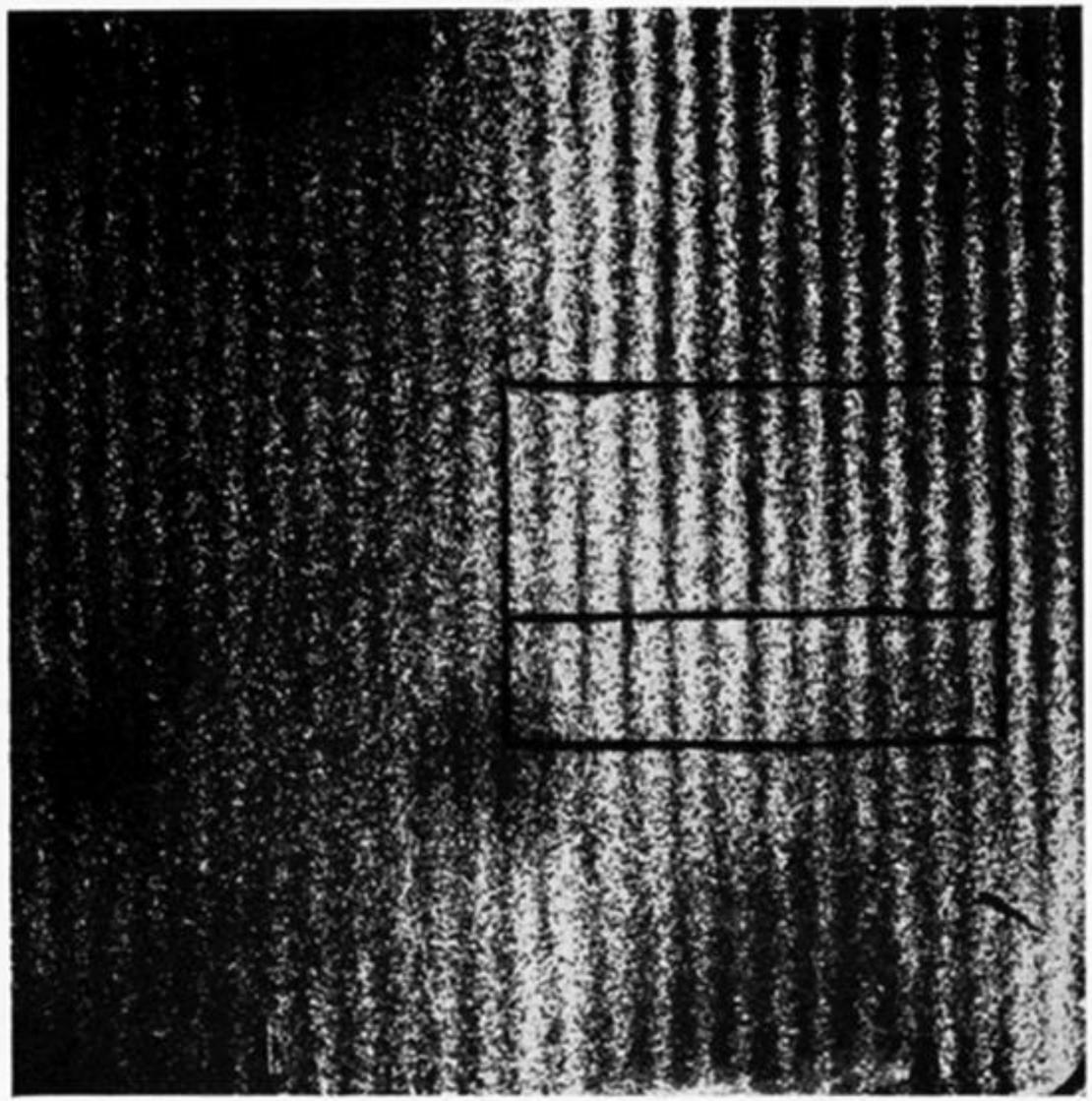

(*a*)

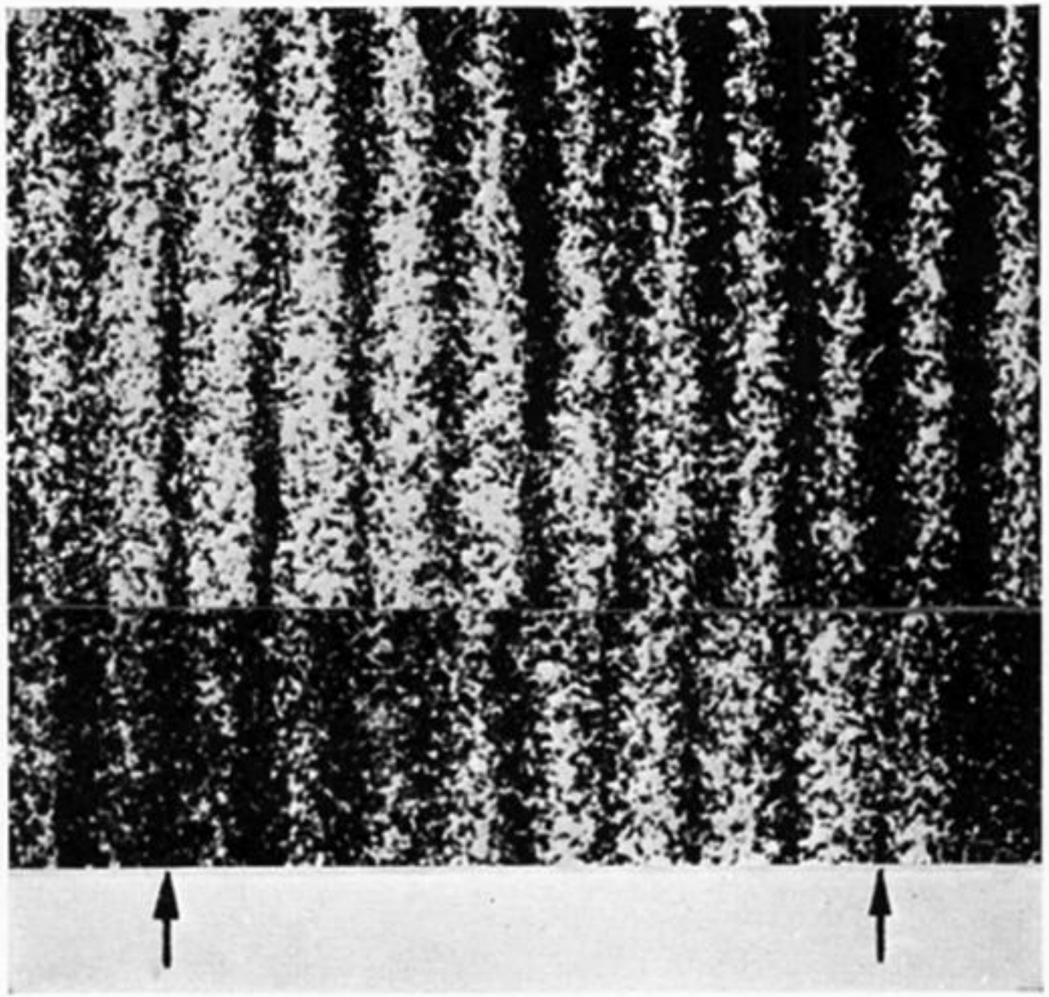

(*b*)

FIGURE 21. (*a*) Electron micrograph of Cu-phthalocyanine showing the spacing anomaly of the fringe. Enlargements (*b*) of enclosed regions, one of which is arranged upside down, indicate that the lines between two lines marked by two arrows shift to each other on both parts of the micrograph. (*a*) Magn. × 2 200 000; (*b*) magn. × 5 000 000. (Courtesy *Nature*, 1959, **183**, p. 1001.)

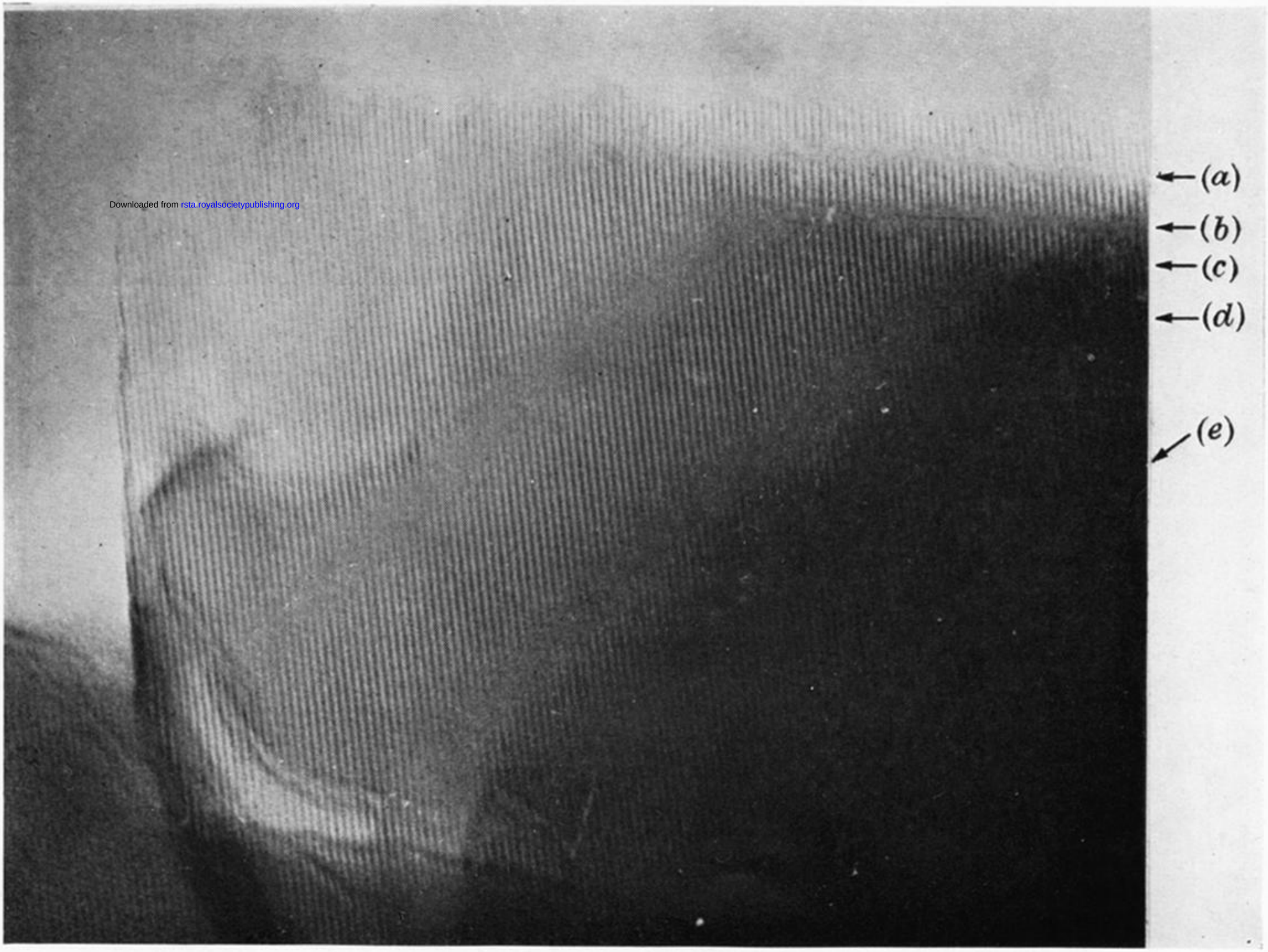

FIGURE 23. Fringe of sodium faujasite showing the stepped structure. By viewing obliquely steps of the fringes are detected along the contours (*a*), (*b*), (*c*), (*d*) and (*e*). (Magn. × 800 000.) (Courtesy J. W. Menter, 1958, *Phil. Mag. Suppl. Advances in Physics*, **7**, p. 132.)